LBNL-39720
UC-404

ERNEST ORLANDO LAWRENCE
BERKELEY NATIONAL LABORATORY

The Crystallography of Fatigue Crack Initiation in Incoloy-908 and A-286 Steel

Christopher R. Krenn
Materials Sciences Division

December 1996
M.S. Thesis

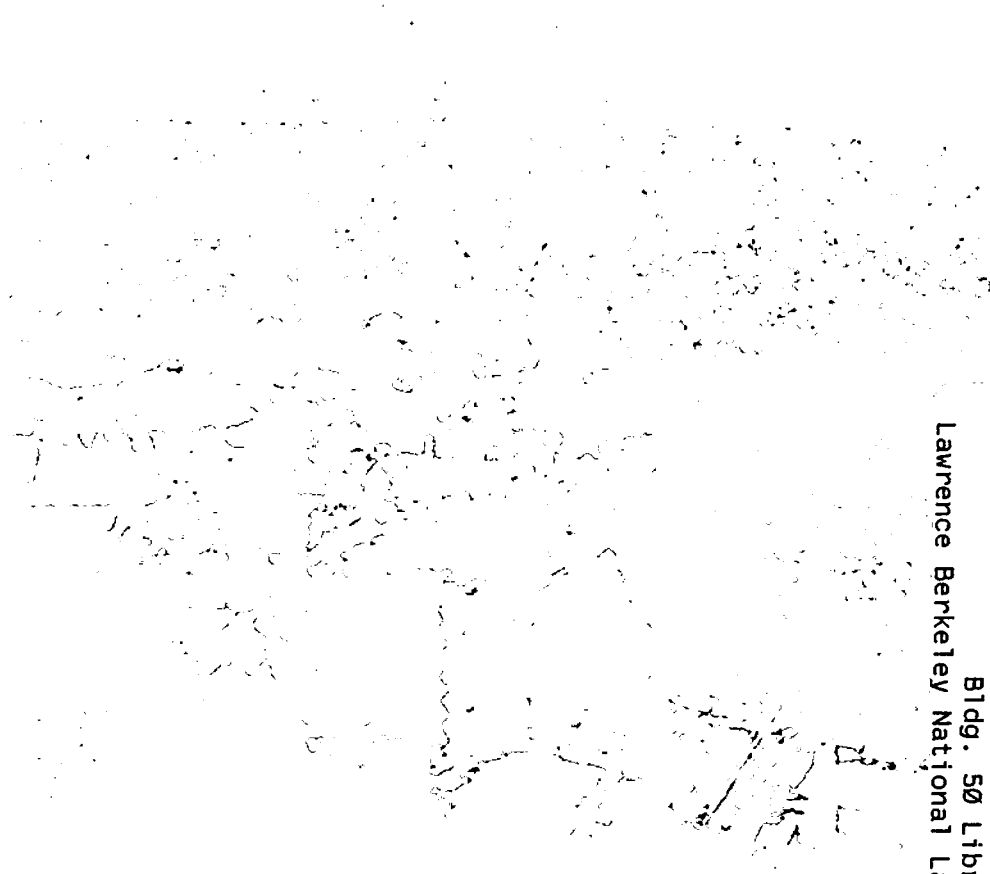

LBNL-39720

DISCLAIMER

LBNL 39720

The Crystallography of Fatigue Crack Initiation in Incoloy-908 and A-286 Steel

M.S. Thesis
of
Christopher R. Krenn

Department of Materials Science and Mineral Engineering
University of California at Berkeley

and

Center for Advanced Materials
Materials Science Division
Lawrence Berkeley National Laboratory
1 Cyclotron Road
Berkeley, CA 94720

December 1996

This work was supported by the Director, Office of Energy Research, Office of Basic Energy Sciences, Division of Materials Sciences, of the U. S. Department of Energy, under Contract No. DE-AC03-76SF00098.

The Crystallography of Fatigue Crack Initiation in Incoloy-908 and A-286 Steel

by
Christopher R. Krenn

Abstract

Fatigue crack initiation in the austenitic Fe-Ni superalloys Incoloy-908 and A-286 is examined using local crystallographic orientation measurements. Results are consistent with sharp transgranular initiation and propagation occurring almost exclusively on {111} planes in Incoloy-908 but on a variety of low index planes in A-286. This difference is attributed to the influence of the semicoherent grain boundary η phase in A-286. Initiation in each alloy occurred both intergranularly and transgranularly and was often associated with blocky surface oxide and carbide inclusions. Taylor factor and resolved shear stress and strain crack initiation hypotheses were tested, but despite an inconclusive suggestion of a minimum required {111} shear stress, none of the hypotheses were found to convincingly describe preferred initiation sites, even within the subsets of transgranular cracks apparently free from the influence of surface inclusions. Subsurface inclusions are thought to play a significant role in crack initiation.

Table of Contents

List of Tables

List of Figures

Acknowledgments

This work was supported by the Director, Office of Energy Research, Office of Basic Energy Sciences, Division of Materials Sciences, of the U. S. Department of Energy, under Contract No. DE-AC03-76SF00098. Time and technical support at two orientation imaging facilities were generously provided by B.L. Adams and K. Kunze, formerly of Brigham Young University, and G.F. Gallegos and E.M. Sedillo of Lawrence Livermore National Laboratory.

I am thankful for the technical assistance of John Jacobsen and Chip Flor among many others at Lawrence Berkeley National Laboratory, and for the advice and the criticism offered by Professors R.O. Ritchie and H.-R. Wenk.

I deeply appreciate the confidence and the freedom my advisor, Professor Morris, has entrusted me with during my studies. I am also grateful for the perspective and encouragement which Zequn Mei, Choongun Kim, Ferdinand Bartels, and Jin Chan have all offered, for Jane Fortado's steady support, for the insightful proofreading by Pete and Carol, and for the continued friendship and support of the many other recent Morris group members: Trey, Dave, Rusty, Ping, Seung-Hyuk, Koji, Chris, Carlos, Heidi, Pamela, and Monica.

My mother and father gave me the confidence and security to succeed in my academic endeavors. My wife, Lilly, gives me much hope for the future.

I. Introduction

Both the commercial iron-based A-286 superalloy and the more recently developed[1,2] nickel-based superalloy Incoloy-908* (I-908) have been candidates for use in structural conduit for high field, superconducting "cable-in-conduit" magnets designed for fusion energy applications. This conduit is a thin walled tube surrounding the niobium-tin or niobium-titanium superconducting cable and serves both as a path for the liquid helium coolant and as a distributed structural element within the magnets' coils.[3,4] Because these conduits have walls as thin as 3-12 mm and are required to support high cyclical Lorentz forces, it is crucial to understand fatigue crack growth in the small crack regime.

Earlier work at Lawrence Berkeley National Laboratory (LBNL) on the fatigue behavior of these alloys[5,6] frequently revealed sharp crystallographic cracking that often paralleled surface slip bands. In addition, the earliest stages of crack growth were very erratic. Cracks grew rapidly across some grains and crept across others. Some grain boundaries stopped cracks altogether, while others barely affected growth at all. The obvious explanation for all of these observations must involve the local crystallographic orientations of individual grains.

Studies of fatigue crack initiation dating back to the 1920s in both single and polycrystalline metals have long associated initiation sites with crystallographic slip and persistent slip bands, stress concentrators, including notches and inclusions, and weakened grain boundaries.[7,8] In early work on the low cycle fatigue of A-286 (typical plastic strains of 1%), Coffin and Solomon[9,10] found nucleation "in all cases occurred on sites of slip band extrusions at the specimen surface." Propagating cracks were observed to be likely to follow growth twin boundaries, but neither observation was directly supported by crystallographic measurements.

More recent work on apparently anomalously fast short crack growth has raised questions concerning such effects as locally fast stress corrosion, closure dependence on plastic wake size and crack torturosity, and the grain-to-grain crystallographic dependence of crack propagation.[11-14] Short fatigue cracks have commonly been observed to initiate and propagate on planes of high shear stress (stage I growth) and later to deviate onto planes with high tensile stresses (stage II).[15,16] Short crack studies also motivated Miller's development of "microstructural fracture mechanics," an attempt to describe the effects of locally inhomogeneous microstructure on fatigue and fracture,[17,18] but very few experimental studies are available that explicitly correlate fatigue crack behavior with local microstructure and crystallography. One exception is the work of Tokaji and collaborators[19,20] that clearly documents fatigue crack retardation at grain boundaries. Tokaji also reported etch pit studies that were consistent with stage I crystallographic shear crack growth on slip planes. Studies on fatigue crack retardation in large-grained aluminum by Chen and Liu[21] showed that a smaller crystallographic misorientation across a grain boundary tended to decrease the

* Incoloy is a trademark of INCO Alloys International, Inc., Huntington, WV.

degree to which the boundary acted as a barrier to fatigue crack growth. Investigations besides these are rare.

Fortunately, advances in microscopy systems and computer-aided indexing techniques are now making it easier to obtain local orientation information. Large grains can be oriented using backscattered Laue diffraction, and both electron channeling and electron backscattered pattern (EBSP) indexing can be used within existing scanning electron microscopes.[22] With local orientation measurements, Adams and Krenn[23,24] could prove that low energy Σ3 coincidence boundaries were significantly less likely to crack under tension in an embrittled alloy of Fe+P, and Davidson and Chan[25] found that high cycle fatigue cracks in a coarse-grained superalloy were most likely to initiate in grains with a low Taylor factor, a measure of the relative ease of slip within a single grain constrained by a polycrystalline matrix. The research reported here uses automated indexing of EBSPs to examine crystallographic effects on fatigue crack initiation and early growth in A-286 and Incoloy-908.

The studies reported here were originally designed to test Davidson and Chan's Taylor factor initiation hypothesis while also examining intergranular initiation and determining what information could be discovered about crystallographic effects on the blunting and retardation of surface cracks at grain boundaries. Those goals proved too optimistic for the data set sizes that were experimentally obtainable. Further work concentrated on obtaining the largest data sets that could be gathered to test transgranular initiation theories in the most statistically reliable manner possible.

II. Experimental Procedure

Fatigue Specimens

Both A-286 and I-908 are austenitic steels hardened by coherent γ' precipitates. I-908 has a slightly higher strength and is designed with a low coefficient of thermal expansion to minimize thermal strains on brittle intermetallic superconductors. As processed, neither alloy had strong crystallographic texture. Table I shows the chemical compositions, Table II describes the thermomechanical heat treatments that parallel the processing steps of multifilamentary Nb_3Sn wire, and Table III lists the tensile properties obtained in previous work.[5,6] The heat treatments steps of I-908 were done in a vacuum furnace with a pressure less than 10^{-6} torr to prevent grain boundary oxidation.

Table I: Chemical compositions of A-286 and I-908

	Composition (Weight Percent)									
alloy	Ni	Fe	Cr	Ti	Mn	Mo	Si	Al	C	Nb
A-286	24.3	bal.	14.6	2.47	0.85	0.11	0.05	0.05	0.05	~
I-908	49.4	bal.	4.09	1.64	3.11	~	~	0.96	0.01	3.11

Table II: Thermomechanical treatments and microstructures of A-286 and I-908

	Thermomechanical Treatment FC: Furnace Cool					γ' Hardening Precipitates	Inclusions	grain size
A-286	20% cold work	200°C 24 hr, FC	340°C 48 hr, FC	660°C 72 hr, FC	725°C 24 hr, FC	$Ni_3(Ti,Al)$	5-10 μm Ti oxide	30 μm-70 μm
I-908	20% cold work	200°C 24 hr	340°C 48 hr	660°C 72 hr	725°C 12 hr, FC	$Ni_3(Ti,Al)$	5-10 μm $(Nb,Ti)_xC_y$	65 μm mean

Table III: Tensile properties* of A-286 and I-908 at 20°C

alloy	Yield (MPa)	Ultimate Strength (MPa)	Uniform Elongation (%)	Total Elongation (%)
A-286	1080	1211	13	20
I-908	1227	1448	8.4	17.9

* Gage length of 1 inch.

The 4-point bending fatigue specimens were rectangular bars with gage length of 20 mm. The first specimens tested measured about 10 by 11 mm in cross section. Later bars measured closer to 6 by 12 mm to maximize the surface area sampled while reducing operating stresses which had fractured several hardened steel pins in the bending rig.

Electropolishing

A critical requirement of using backscattered electron diffraction to measure local orientation is for the surfaces of interest to be sufficiently free of deformation to allow diffraction patterns to be obtained. For most metals, even the residual deformation from diamond polishing obscures the patterns, and electropolishing is required. Several commercial electropolishing systems are available, but none could smoothly polish the relatively large areas of the specimens used in this study, and an original system was designed.

Electropolishing works by preferentially dissolving high points of a surface. A specimen is made the anode of a suitable electrolytic cell, and, at a certain range of potentials, a viscous reaction film forms on its surface. Since there is a significant potential drop through this film, regions of the specimen closer to the surface of the film are dissolved more quickly than the bulk, and the specimen becomes increasingly smooth.[26] Electropolishing is therefore an ideal method for eliminating residual surface roughness and deformation.

Several trial runs isolated two significant obstacles to an effective polish: turbulence in the electrolyte and transient pitting before the reaction film developed. The turbulence was addressed by building a rigid specimen holder that could be smoothly lowered into a large stirred bath of electrolyte chosen in previous studies on I-908: 70 parts ethanol, 14 parts water, 10 parts 2-butoxyethanol, and 6.2 parts perchloric acid.[2] Since butoxyethanol was used to make the solution more viscous, a thin layer of pure butoxyethanol on the surface of the specimen was correctly reasoned to protect the surface from pitting until the reaction film could form. This was originally done from a squeeze bottle, but to increase reliability, 5 nozzles were added to the design. A well-sanded thin copper strip insuring good electrical contact completed the design as shown in Figure 1.

Each specimen was mechanically polished to 1μm and then electropolished for 15 seconds at 40 volts. Etching in a fresh solution of 15 parts nitric acid, 45 parts 37% hydrochloric acid, and 20 parts methanol for 25 seconds revealed grain boundaries.

Fatigue Testing and Crack Mapping

As in previous LBNL studies,[5,6] the polished and etched smooth bar specimens were tested in air at room temperature under load control on a hydraulic testing machine using the four-point bending configuration diagrammed in Figure 2. The applied load was a 5 Hz haversine with a load ratio R ($=P_{min}/P_{max}$) of 0.05. The maximum applied surface stress,

$$\sigma_{max} = \frac{3P_{max}a}{bh^2} \qquad [1]$$

was 90% of the bulk yield to insure initiation of a large sample of cracks. Acetate replicas of the tensile surface were taken every 5000 cycles to locate and monitor initiation sites.

The tests were stopped when a significantly long crack was visually detected and assumptions of constant surface stress no longer held. A 50x magnification photographic montage was created to record crack position, and cracks were indexed by visually scanning the entire gage area at 400x in a polarized binocular microscope. This technique allowed interactions between neighboring cracks to be recognized and the Cartesian coordinates of cracks of interest to be recorded to allow them to be quickly located in an SEM. Calibrated specimen holders allowed gold-plated replicas to be scanned quickly to determine initiation sites of longer cracks.

Orientation Imaging

Venebles and Harland[27] first described using electron back-scattering patterns (EBSPs) to obtain crystallographic information in the scanning electron microscope (SEM). Analysis of patterns imaged on a phosphor screen mounted in the SEM can reliably fix specimen orientation to within 2°. This study uses a system based on one described by Dingley and Baba-Kishi[28] and automated by Wright and Adams.[29,30] This "orientation imaging microscope", which allows the rapid on-line analysis of EBSPs, has been commercialized by *TexSEM* Laboratories* and has stimulated the development of a similar system at the University of California at Berkeley.[31]

Individual grain orientation measurements were made at two *TexSEM* facilities: one at Brigham Young University and a second at Lawrence Livermore National Laboratory.

Numerical Analysis

From the raw orientation data, it was possible to calculate several parameters of interest, including measures of lattice uniformity, descriptions of possible crack planes, and the relationships between crystallographic slip planes, the specimen surface, and the applied stress:

The misorientation between two lattices can be reduced to a fixed rotation about a single axis. The minimum such rotation, accounting for the indistinguishability of cubic <100> axes, was calculated as a measure of the lattice deformations between several points within a single seemingly uniform grain as defined by optical microscopy and chemical etching. Misorientation measurements also served as a check to determine whether apparent transgranular cracks as determined from replica examination were in fact intergranular. The FORTRAN code is listed in the appendix.

It is impossible to determine the crack plane from only lattice orientation information and observations of a polished surface. However, these measure-

* TexSEM is a trademark of TexSEM Labs. Inc., Provo, UT.

ments restrict the possible planes on which an observed crack can lie to a set with a single degree of freedom: rotation about the trace the crack makes along the surface. A program was written in *Mathematica* to plot the possible *ijk* components of a given crack plane using the following formula:

$$[ijk] = \left| \overline{nd} \cdot Sin\beta + \left(\overline{nd} \times \overline{cd} \right) \cdot Cos\beta \right| \qquad [2]$$

In a crystallographic frame of reference, $\overline{nd}$** is the surface normal and the cross product $\overline{nd} \times \overline{cd}$ is perpendicular to the crack line. β measures the angle the plane makes with the surface.

Similar formulae calculate the angle α between the crack trace and the tensile direction, the angle β between a given plane and the plane of the surface, and the angular deviation Δ between observed crack lines and the intersection of a plane $\{ijk\}$ with the surface:

$$\begin{aligned} \alpha &= ArcCos\left(\overline{cd} \cdot \overline{td} \right) \\ \beta &= ArcSin\left(\{ijk\} \cdot \overline{nd} \right) \\ \Delta &= ArcCos\left(\overline{cd} \cdot \left(\overline{nd} \times \{ijk\} \right) \right) \end{aligned} \qquad [3]$$

These angles are shown in Figure 3. When angular deviations or stresses were calculated for a crystallographic family of planes such as {111}, calculations were made for all planes belonging to the family, and the maximum stress or minimum deviation reported. Finding the distribution of deviations Δ between a crack trace and a given crystallographic plane significantly lower than the distribution from a randomly oriented sample provides strong evidence for a common crystallographic crack plane.

Shear stresses and strains were referenced to an applied unit stress or strain of 1.0. The maximum shear stress on a {111} plane could range from 0.33 to 0.5, while the maximum shear strain could range from 0.67 to 1.0.

Finally, assuming {111} slip as the only mode of deformation, plane strain Taylor's factors were calculated (following Bishop and Hill[32,33]) as a measure of the ease of constrained deformation within the polycrystalline matrix. In the case of the uniaxial, plane strain loading that holds for 4-point bending, the Taylor's factor is the ratio between the applied stress and the resolved shear stress on the active slip systems and can vary from a minimum of 2.0 to a maximum of 4.9. This FORTRAN code is also listed in the appendix and produces results consistent with G.Y. Chin and D.L. Davidson.[25,34]

** *nd*, *td*, and $\overline{rd}$ will consistently stand for the normal, transverse (tensile), and rolling directions of the specimen in the crystallographic frame of the grain of interest. $\overline{cd}$ similarly will define the direction of the visible line of the crack on the surface.

In most cases, numerical analysis of experimental data was repeated on a statistically large representational set of "random" grains to determine the statistical relevance of conclusions made. A set of 72 surface normal *nd* orientations that spanned two <100><101><111> crystallographic unit triangles was chosen such that each point was associated with an angular area of approximately 25 degrees^2, as shown in Figure 4. Because of the additional degree of freedom of rotation of the tensile and transverse directions around the normal direction, this set of 72 is further multiplied by a factor of 9 to uniformly span the remaining space in increments of 5°. To compare data sets of different sizes, distributions were plotted on linear probability paper.

III. Experimental Results

Preliminary Results: Incoloy-908

Only two complete sets of fatigue crack testing, mapping, and orientation imaging experiments were possible within the scope of this research. A specimen of I-908 was fatigued to 23,000 cycles before a significant edge crack was detected. Optical micrographs (Figures 5(a)-5(e)) document the variety of cracks found. Cracks propagated both intergranularly and transgranularly, along apparently sharp crystallographic directions and along tortuously curved paths. Blocky inclusions and occasional persistent slip bands appear to affect both initiation and propagation. Using EBSP indexing techniques, the orientations of 132 grains bounding 20 cracks of varying lengths were measured.

As acknowledged earlier, hopes to examine transgranular and intergranular initiation as well as grain boundary blunting were too optimistic. Since the initiation and propagation behavior of short cracks is largely statistical in nature, to discover significant trends in the data required more than the two or three examples of each simple class of crack that could be observed in the microscope time available. The large number of parameters defining each crack made it impossible to make any useful conclusions about intergranular initiation sites or about grain boundary retardation of fatigue cracks. In addition, with only one exception, all of the transgranular crack initiation sites occurred near large blocky inclusions which greatly complicated the calculation of local resolved stresses and Taylor factors.

Still, the data offered some information about fatigue crack initiation sites (Table V), and a discrete pole figure plot (Figure 6) showed that there is no apparent strong preferred orientation texture among the 132 grains measured (including sites of transgranular initiation, blunting sites, and sites bounding intergranular cracks). Pole figures of each subset did not expose any preferred orientations.

Significantly, it was possible to confirm that almost all of the sharp crystallographic crack growth in I-908 was consistent with {111} growth. 8 out of 9* measured crack segments lay within 4° of the intersection of a {111} plane and the surface. Figure 7 shows the deviations between a fixed surface trace and the nearest {111} plane for both these observed cracks (omitting the single outlier) and a randomly oriented sample. Two surface slip bands also lay within 2° of {111} planes. The only plausible reason why the population of crack traces was so close to the intersection of {111} planes and the surface is that cracking occurred almost exclusively on {111} planes.

Detailed analysis of the three observed transgranular initiation sites was performed in order to justify further measurements (see Table IV). Only the one crack (Figure 5(e)) that did not initiate near an inclusion was easily correlated to

* From a plot of the possible normals of the remaining crack, it seems most likely to be {100}, or given the more detailed analysis of A-286 data, it is also possible it is a low energy grain boundary which was not revealed by etching.

any simple initiation model. This crack apparently occurred on a {111} plane whose trace on the surface made an angle of 38° with the tensile direction, and within measurement accuracy, this plane was perfectly perpendicular to the surface. Although the Taylor factor for this grain was not particularly low, the resolved shear stresses and strains on this plane are almost the maximum possible.

Table IV: Analysis of fatigue crack initiation sites in I-908

	α	β	resolved shear σ	resolved normal σ	Taylor factor
no inclusion	38	90	0.499	0.470	2.88
inclusion A	58	61	0.247	0.065	3.31
inclusion B	35	72	0.437	0.740	3.40
maximum*	90	90	0.500	1.000	4.89
minimum*	0	0	0.000	0.000	2.00
random average**	45	36	0.487	0.471	3.45

α=angle between surface trace and tensile direction
β=angle between {111} crack normal and surface normal

* the maximum, minimum and "random" values of α, β, and the resolved stresses are calculated for the {111} plane with the highest resolved shear stress.

** Davidson and Chan[25] cite the average value of this plane strain Taylor factor as 3.53, but because the steepness of the gradient of M in some parts of the unit triangle, the calculation depends significantly on the details of the geometric averaging used.

Initiation Studies: A-286

Optical microscopy

A-286, the other "cable-in-conduit" candidate alloy of interest in past fatigue studies at LBNL, was chosen for a second round of experiments to complement earlier work[5,6] and, because preliminary studies suggested that a high fraction of transgranular initiation sites could be found without inclusions, to provide a good test of transgranular initiation theories. The goal in these experiments was to find at least 15 transgranular initiation sites as well as 15 blunting sites (sites believed to be relatively poorly oriented for crack initiation) to rigorously test Davidson and Chan's Taylor factor initiation theories. The work was then planned to be extended to examine cracks near blocky inclusions. Finally, the crystallography of observed crack planes would be tabulated.

A specimen of A-286 was fatigued to 70,000 cycles before cracking became visually apparent. Cracking modes (as shown in the micrographs in Figure 8) were similar to I-908, but a larger population was initiated. A detailed survey of the surface identified 90 cracks in the first 20% of the gage section. This sample was judged more than large enough to produce reasonable statistics, and 45 of these cracks were chosen randomly by computer for initiation site determination using acetate replicas. Sites were classified as intergranular or transgranular, and the existence of inclusions within a one-grain radius of the initiation site was also

noted (Table V presents these statistics, with "isolated" meaning "having no nearby surface inclusion"). Since only transgranular initiation theories were of interest and because the initiation sites of long cracks were difficult to determine, the remaining 80% of the gage section was scanned for shorter cracks that did not apparently initiate intergranularly (Figure 9 shows all mapped cracks). The right end of the specimen did have a greater number of cracks in total because of the stress increases caused by several long cracks, but those cracks where initiations were clearly influenced by existing crack stress fields were excluded from detailed crystallographic initiation analyses.

Table V: Statistics of fatigue crack initiation sites in A-286 and I-908

I-908	A-286	
16	42	initiation sites determined from replicas
25	40	% isolated intergranular
6	10	% isolated transgranular
25	36	% intergranular near visible inclusion
44	14	% transgranular near visible inclusion
50/50	76/24	% intergranular/transgranular
31/69	50/50	% isolated/near inclusion

Orientation imaging

Grains surrounding 32 crack sites were categorized into three sets for crystallographic analysis: transgranular initiation sites with and without nearby surface inclusions, and "blunting sites": grains that resisted crack propagation. Inverse pole figures (Figure 10) of each set failed to reveal any groupings considered significant, despite the apparent sparsity of points along the (100)-(101) axis for the tensile directions of blunting sites and along the (100)-(111) axis for the normal directions of grains containing isolated transgranular cracks. A discrete pole figure plot of all grains measured (Figure 11) did not reveal any significant overall texture.

The lattice misorientation across each crack of interest was measured. Misorientations calculated from 6 measurements in an incompletely cracked grain (Figure 12 shows their geometry and magnitudes) ranged from 4° to 7° and suggest that misorientations of less than 10° can be attributed to the inhomogeneity of the lattice and errors in the automatic indexing. A histogram of misorientation rotations across all measured cracks (Figure 13) revealed that a significant number of the cracks classified as transgranular from replica observations were, in fact, intergranular. The distribution was bimodal. Misorientations near 5° were confirmed as describing transgranular cracks and misorientations near 55° (potentially low energy twin boundaries not revealed by etching) reclassified as describing intergranular cracks (Table V reflects these corrections).

Crack plane analysis

To search for low index cleavage or slip planes intersecting crack traces on the surface (not always in grains of initiation, but always in the short crack regime), the absolute values of *i, j,* and *k* defining possible plane normals {*ijk*} were plotted as a function of the angle the plane made with the surface. Reference lines in the plot mark the first and last 10° from the surface as well as the 90° perpendicular. These plots were designed to quickly reveal {111}, {100}, and {110} planes; a triple intersection of *i, j,* and *k* (within a 5-10° error ellipse) reveals a {111} plane, and {110} and {100} planes can be similarly recognized. The normal of a plane passing through the crack trace at any given angle beneath the surface is defined by the intersection of a vertical line with the *i, j,* and *k* curves. Figure 14(a) shows a grain with a surface normal very close to {100} where two {111} planes and one {110} plane pass through the trace of the crack on the surface, while Figure 14(b) depicts a grain in which {100} is the only low index plane that intersects the crack trace.

Visual analysis of these plots for all 25 observed sharp transgranular cracks in A-286 (Figure 15) revealed that the large majority were consistent with low index crystallographic growth, but only a minority were consistent with the typical {111} growth visible in the crack plane plots of I-908 (Figure 16). Table VI summarizes the visual analysis for both alloys:

Table VI: Analysis of crystallographic planes intersecting crack traces in A-286 and I-908

	Crack traces lying near low index planes*							
	at least 1 plane			at least 2 planes				
alloy	111	100	110	111/100	111/110	100/110	all 3	none
A-286 (n=25)	36%	52%	52%	12%	4%	24%	8%	12%
I-908 (n=9)	89%	22%	11%	22%	11%	0%	0%	0%

* This visual analysis ignored planes within 10° of the surface that were judged unlikely to have cracked.

The three apparently sharp crystallographic cracks in A-286 that did not have low index planes passing through their surface traces were initially puzzling. However, in all cases, these cracks were not in grains of initiation, but within the second grain of crack propagation. In one case, there was a {111} plane just under 10° from the surface, and in the other two, the crack direction paralleled closely the crystallographic direction in the grain of initiation. Growth proceeded not because of weakness in the observed grain, but because of the potency of the notch formed in an adjacent grain.

As with I-908, the validity of these observations was tested by comparing the deviations of the observed crack traces from low index planes to the deviations calculated from a random sample (Figure 17). Though the deviations do not appear significantly smaller than the random set, they do mostly lie within measurement error. These experiments show that cracking does not generally occur on {111} planes in A-286, but can neither confirm nor deny propagation on other low index planes.

IV. Discussion

Crystallography of Transgranular Cracks

The experimental observations of short transgranular cracks in I-908 were consistent with sharp stage I shear growth on {111} planes. The one exception to this {111} growth as seen in the crack plane plot (Figure 16) is crack 5d (the lower crack in Figure 5(c)). This crack initiated at a blocky inclusion and appears to propagate along a {100} plane oriented nearly perfectly perpendicular to the applied stress: theoretically ideal for a stage II tensile crack. Three conspicuous slip bands were analyzed and were of note for the crystallographic symmetries apparent in a crack plane plot. Both grains 2a and 2b (an optical micrograph of 2b is attached as Figure 5(a)) had {110} surface normals and two symmetric {111} planes passing through the slip lines visible on the surface. The family of parallel slip lines perpendicular to the long isolated transgranular crack visible in Figure 5(e) also had two symmetric intersecting {111} planes. (In Figure 16, the main crack is identified as 24a, and the slip line trace as 24a2.) These symmetries were not investigated more rigorously because of the many cracks observed to initiate without the benefit of such orientation relations.

Despite having a crystal structure, grain size, and distribution of precipitates and inclusions very similar to I-908, in A-286 only a minority of observed crack on {111} slip planes. The most plausible explanation for this difference involves the Ni_3Ti η phase. This has previously been observed to appear in A-286 by precipitation at grain boundaries after overaging heat treatments at 720°C for times exceeding 6 hours.[35,36] As the specimens tested in this study were treated for 24 hours at 725°C, submicron, semi-coherent, disk shaped η was most likely present at the grain boundaries, although it was not observed by optical microscopy. Fatigue crack initiation has been observed at micron scale cellular η colonies in highly overaged (100°C for 100 hours) A-286;[37] smaller sized colonies could reasonably influence the plane of crack initiation.

Since the habit plane of η is {112},[36] the crack traces of all 24 sharp segments in A-286 were reanalyzed with respect to {112} initiation. Although 75% of traces lay within 10° of one of the 12 {112} planes as compared to 41% of traces that lay near one of the 4 {111} planes (25% of traces lay more than 10° from either type of plane), comparison of the cracked deviations to the random set (Figure 18) shows that, due to the larger number of {112} planes, this is not statistically significant. This does not completely discount the influence of coherent η, however. Cracks could initiate at the {112} interface between η and the matrix, and then, depending on the local stress state, quickly deviate onto another low index plane.

A second mechanism for the precipitation of η is the growth of cellular colonies from grain boundaries. These appear as alternating lamellae which have random orientation relationships with the grains into which the cellular zones grow.[38] Interface failures in these colonies can also inject cracks into the austenitic matrix. The almost complete uniformity of {111} cracking in I-908 is in either case understandable because I-908 was designed to be stable against overaging and the formation of η for heat treatments of up to 100 hours at tempera-

tures of 750°C.[2] Without grain boundary η to serve as crack nucleation sites, cracks will nucleate at the next most potent source of stress concentration: {111} persistent slip bands.

Characterization of Crack Initiation Sites

One of the major goals of this research was to identify the crystallography of statistically weak regions of the microstructure that were most likely to initiate fatigue cracks. Table V showed that two of the most significant weaknesses in both I-908 and A-286 were grain boundaries and large inclusions. The influence of inclusions is also underreported because subsurface inclusions were not detected. Therefore, two goals of particular engineering relevance would be to characterize grain boundary crack initiation and to probe the mechanisms by which isolated inclusions can inject cracks into neighboring grains. However, grain boundary initiation depends strongly on the orientation of the boundary plane with respect to the surface, and initiation near blocky inclusions depends strongly on local stress concentrations.

Because boundary orientations and stress concentrations are very difficult to determine experimentally, previous experience characterizing intergranular fracture sites[23,24] suggested to first attack the more scientifically tractable problem of isolated transgranular initiation. This required searching for uniqueness amidst a data space spanned by only 3 Euler angles, as opposed to the 8 dimensional data space required to fully define a crystallographic interface that is externally stressed.* In addition, the most important variables in this case are the local stress state and the grain orientation. It is reasonable to assume that surface orientation measurements can accurately represent the entire volume of a grain, and, isolated from inclusions, local stresses will be close to the macroscopic averages.

Since most studies on single crystals and smooth uniform polycrystalline specimens in both high (macroscopically plastic) and low (macroscopically elastic) stress regimes have associated transgranular crack initiation with slip band and extrusion formation, Davidson and Chan's hypothesis that polycrystalline initiation is most likely to occur in grains with low Taylor factors is plausible. A grain with a low Taylor factor is well oriented for multiple slip within the constraints of an elastic matrix; it can therefore be subjected to cyclical plastic deformation while the majority of the bulk is still purely elastic. However, for A-286, a plot comparing the distributions of calculated Taylor factors for cracked grains, blunting sites, and the random set revealed no statistically significant differences (Figure 19). The simplicity of the Davidson-Chan theory was most likely overshadowed by the complexity of the alloy systems examined and is further challenged by reported TEM observations in a 32Mn-7Cr austenitic steel[39] which found very little secondary slip activity during high cycle fatigue.

* 3 Euler angles are necessary to de4fine a crystallographic orientation with respect to a laboratory reference frame. An interface requires information about the orientations of both grains (6 angles as well as the plane of the interface (2 more angles).

These TEM studies suggest that Taylor's deformation model, which requires multiple slip to accommodate tensile deformation, might not entirely hold during fatigue with only slight localized plasticity.

Initiation hypotheses suggested by the research reported here were based on an initial assumption that the one isolated transgranular crack in I-908 had an almost ideally weak orientation. Since only one grain out of the tens of thousands surveyed cracked without the benefit of a stress raising inclusion or other flaw, its orientation was believed to be correspondingly unique, including, most obviously, an extremely high {111} shear stress. Initial analysis of the maximum resolved shear stresses on {111} planes in A-286 revealed one promising difference in the distributions from cracked and uncracked grains (Figure 20): the lower end of the distribution of isolated transgranular cracks seemed to be significantly greater than those of both blunting sites and cracks initiated near inclusions. This could suggest that a necessary, but not sufficient, condition for crack initiation would be a certain critical {111} shear stress. However, since the portion of the distributions in question only represents 2-3 data points in each set, this conclusion can not be firmly established.

A second piece of data suggests why a stress criterion might not apply to the cracks observed in this study. Surface crack traces tended to lie roughly 45° away from the direction of applied stress (Figure 21 is a histogram of this angle α). In the specimen geometry used, stress is uniaxial, and resolved shear stress is only a function of the angle between the crack normal and the tensile direction and does not predict this clustering of α's. A crack with α=45° that was also perpendicular to the surface would have the same resolved shear stress as a crack whose surface trace was perpendicular to the loading direction (α=90°) that intersected the surface with an angle of 45°.

Using a plastic plane strain criterion, as used by Miller in his work on multiaxial fatigue,[40-42] uniquely defines two planes with maximal shear strain: both perpendicular to the surface with $\alpha=\pm 45°$. Postulating that cracks are most likely to initiate on planes of maximum shear strain is consistent with both the orientation of the "ideally weak" isolated transgranular I-908 crack (which has an almost ideally high resolved shear strain) and the observed clustering of crack traces near 45° away from the tensile axis. However, a final plot comparing the distributions of these {111} shear strains in A-286 revealed no significant differences between the populations of grains observed (Figure 22).

V. Conclusions

After preliminary studies were completed in Incoloy-908, three hypothetical criteria of isolated transgranular fatigue crack initiation were investigated in the superalloy A-286. Observed crack initiation sites had neither markedly low Taylor factors nor notably high resolved shear stresses or strains on {111} planes. The rarity of crack initiation sites not closely associated with blocky inclusions (9 sites out of almost 100,000 observed grains) was initially thought to suggest particularly severe crystallographic weakness, that these grains were oriented extremely favorably for crack initiation. However, as several thousand significant inclusions were observed on the surface, this same rarity could also associate each crack site with a large subsurface inclusion. A valid test of transgranular initiation theories would require an alloy system without blocky inclusions and perhaps a better understanding of the ways in which such features as grain boundaries, triple points, and local microtexture can affect local stress and strain states.

The majority of crystallographically sharp stage I shear cracks in A-286 did not lie on {111} planes, while almost all of the limited number analyzed in I-908 did. This is particularly significant because these observations refute the firm association in the fatigue literature between sharp shear cracking and crystallographic slip planes. Observations of shear fatigue crack growth in single crystals have suggested that short shear crack growth in polycrystals will occur on the slip planes of each individual grain. While this appears to be true in Incoloy-908, the presence of grain boundary η phase was theorized to explain why this did not hold in A-286. Crystallographic measurements of cracked grains in A-286 were consistent with low index crack growth on {100}, {110}, and {111} planes but could not conclusively prove such growth. Better understanding of these results demands transmission electron microscopy of fatigue initiation sites to determine the role, if any, of the η phase. Crack plane measurements by serial sectioning or precision dimpling could document low index growth definitively.

After the processing necessary for superconducting magnetic coil fabrication, grain boundaries and blocky inclusions were found to be the most potent fatigue crack initiation sites in the two complex engineering alloys A-286 and I-908 Although this work does not suggest any clear methods of improving fatigue behavior of austenitic superalloys, it is apparent from the observations of grain boundary initiation, previously investigated initiation from cracked and debonded inclusions, and the possibly significant influences of grain boundary phases on transgranular initiation, that further study of interfacial fatigue promises to be fertile.

References

1. M.M. Morra, I.S. Hwang, R.G. Ballinger, M.M. Steeves, and M.O. Hoenig: *11th International Conference on Magnet Technology (MT-11)*, 1990, vol. 1, pp. 731-6.
2. M.M. Morra, R.G. Ballinger, and I.S. Hwang: *Metall. Trans. A*, 1992, vol. 23, pp. 3177-92.
3. *Magnet Design Technical Report: ITER Definition Phase*, C. Henning, ed., Lawrence Livermore National Laboratory, Livermore, CA, 1989.
4. L.T. Summers, J.R. Miller, and J.R. Heim: *Adv. Cryo. Eng.*, 1990, vol. 36, pp. 769-76.
5. Z. Mei and J.W. Morris, Jr.: *Metall. Trans. A*, 1993, vol. 24A, pp. 689-701.
6. Z. Mei, C.R. Krenn, and J.W. Morris, Jr.: *Metall. Mater. Trans. A*, 1995, vol. 26A, pp. 2063-73.
7. C. Laird and D.J. Duquette: in *Corrosion Fatigue : Chemistry, Mechanics and Microstructure*, A.J. McEvily, R.W. Staehle, and O.F. Devereux, eds., NACE, Houston, TX, 1972, pp. 88-117.
8. S. Suresh: *Fatigue of Materials*, Cambridge University Press, Cambridge, 1991.
9. L.F. Coffin, Jr.: *Metall. Trans. A*, 1972, vol. 3, pp. 1777-88.
10. H.D. Solomon: *Metall. Trans. A*, 1973, vol. 4, pp. 341-7.
11. S. Suresh and R.O. Ritchie: *Int. Met. Rev.*, 1984, vol. 29, pp. 445-76.
12. *Small Fatigue Cracks: Proceedings of the Second Engineering Foundation International Conference*, R.O. Ritchie and J. Lankford, eds., Metallurgical Society, Warrendale, PA, 1986.
13. *The Behaviour of Short Fatigue Cracks*, K.J. Miller and E.R. De los Rios, eds., Mechanical Engineering Publications, London, 1986.
14. *Short Fatigue Cracks*, K.J. Miller and E.R. De los Rios, eds., European Structural Integrity Society, London, 1992.
15. P.J.E. Forsyth: in *Proceedings of the Crack Propagation Symposium*, The College of Aeronautics, Cranfield, England, 1961, pp. 76-94.
16. K.J. Miller: in *Fundamentals of Deformation and Fracture*, B.A. Bilby, K.J. Miller, and J.R. Willis, eds., Cambridge University Press, Cambridge, 1985, pp. 477-500.
17. K.J. Miller: *Mater. Sci. Technol.*, 1993, vol. 9, pp. 453-62.
18. K.J. Miller: *Fatigue Fract. Eng. Mater. Struct.*, 1993, vol. 16, pp. 931-9.
19. K. Tokaji, T. Ogawa, and S. Osako: *Fatigue Fract. Eng. Mater. Struct.*, 1988, vol. 11, pp. 331-42.

20. K. Tokaji and T. Ogawa: in *Short Fatigue Cracks*, K.J. Miller and E.R. de los Rios, eds., Mechanical Engineering Publications, London, 1992, pp. 85-99.

21. Q. Chen and H.W. Liu: *Scripta Metall. Mater.*, 1993, vol. 28, pp. 849-52.

22. V. Randle: *Microtexture Determination and Its Applications*, The Institute of Metals, London, 1992.

23. B.L. Adams: *Mater. Sci. Eng. A*, 1993, vol. A166, pp. 59-66.

24. C.R. Krenn: *Senior Thesis*, Yale University, New Haven, CT, 1992.

25. D.L. Davidson and K.S. Chan: *Acta Metall.*, 1989, vol. 37, pp. 1089-97.

26. *ASM Metals Handbook*, American Society for Metals, Metals Park, OH, 1973, pp. 26-33.

27. J.A. Venables and C.J. Harland: *Phil. Mag.*, 1973, vol. 27, pp. 1193-200.

28. D.J. Dingley and K. Baba-Kishi: *Scanning Electron Microscopy*, 1986, pp. 383-91.

29. S.I. Wright and B.L. Adams: *Metall. Trans. A*, 1992, vol. 23A, pp. 759-67.

30. B.L. Adams, S.I. Wright, and K. Kunze: *Metall. Trans. A*, 1993, vol. 24A, pp. 819-31.

31. H.-R. Wenk, G.C. Johnson, J.W. Morris, Jr., and P.J.M. Monteiro: *Proposal to the National Science Foundation*, University of California, Berkeley, 1995.

32. J.F.W. Bishop and R. Hill: *Phil. Mag.*, 1951, vol. 42, pp. 1298-307.

33. J.F.W. Bishop and R. Hill: *Phil. Mag.*, 1951, vol. 42, pp. 414-27.

34. G.Y. Chin and W.L. Mammel: *Trans. TMS-AIME*, 1967, vol. 239, pp. 1400-5.

35. J.A. Brooks and A.W. Thompson: *Metall. Trans. A*, 1993, vol. 24A, pp. 1983-91.

36. R.F. Decker and S. Floreen: in *Precipitation from Iron-base Alloys*, G.R. Speich and J.B. Clark, eds., Gordon and Breach Science Publishers, New York, 1965, pp. 69-139.

37. M.A. Daeubler, A.W. Thompson, and I.M. Bernstein: *Metall. Trans. A*, 1991, vol. 22, pp. 513-19.

38. D.R. Muzyka: in *The Superalloys*, C.T. Sims and W.C. Hagel, eds., Wiley-Interscience, New York, 1972, p.125.

39. O. Umezawa and K. Ishikawa: *Adv. Cryo. Eng.*, 1992, vol. 38, pp. 141-8.

40. K.J. Miller: *J. Mater.*, 1972, vol. 7, pp. 307-14.

41. K.J. Miller: *Metal Science*, 1977, vol. 11, pp. 432-8.

42. K.J. Miller and M.W. Brown: in *Advances in Fracture Research (Fracture 84). Proceedings of the 6th International Conference on Fracture (ICG6)*, S.R. Valluri, ed., Pergamon Press, New York, 1986, pp. 31-56.

Colophon

Production of this thesis was made possible by the following:

Hardware

Apple Macintosh LC III personal computer, Umax scanner, and APS tape and hard drives.

Software

Microsoft Word 5, Endnote Plus, Word Ref, Microsoft Excel 4, KaleidaGraph, Mathematica, Language Systems MPW Fortran, Canvas, AutoCAD, and the UC Melvyl and Inspect databases.

Inspirational Reading

M.M. Waldrop: *Complexity: The Emerging Science at the Edge of Order and Chaos,* Simon & Schuster, New York, 1992.

E.R. Tufte: *The Visual Display of Quantitative Information,* Graphics Press, Cheshire, CT, 1983.

R. Rhodes: *The Making of the Atomic Bomb,* Simon & Schuster, New York, 1986.

J.K. Conway: *True North,* A.A. Knopf, New York, 1994.

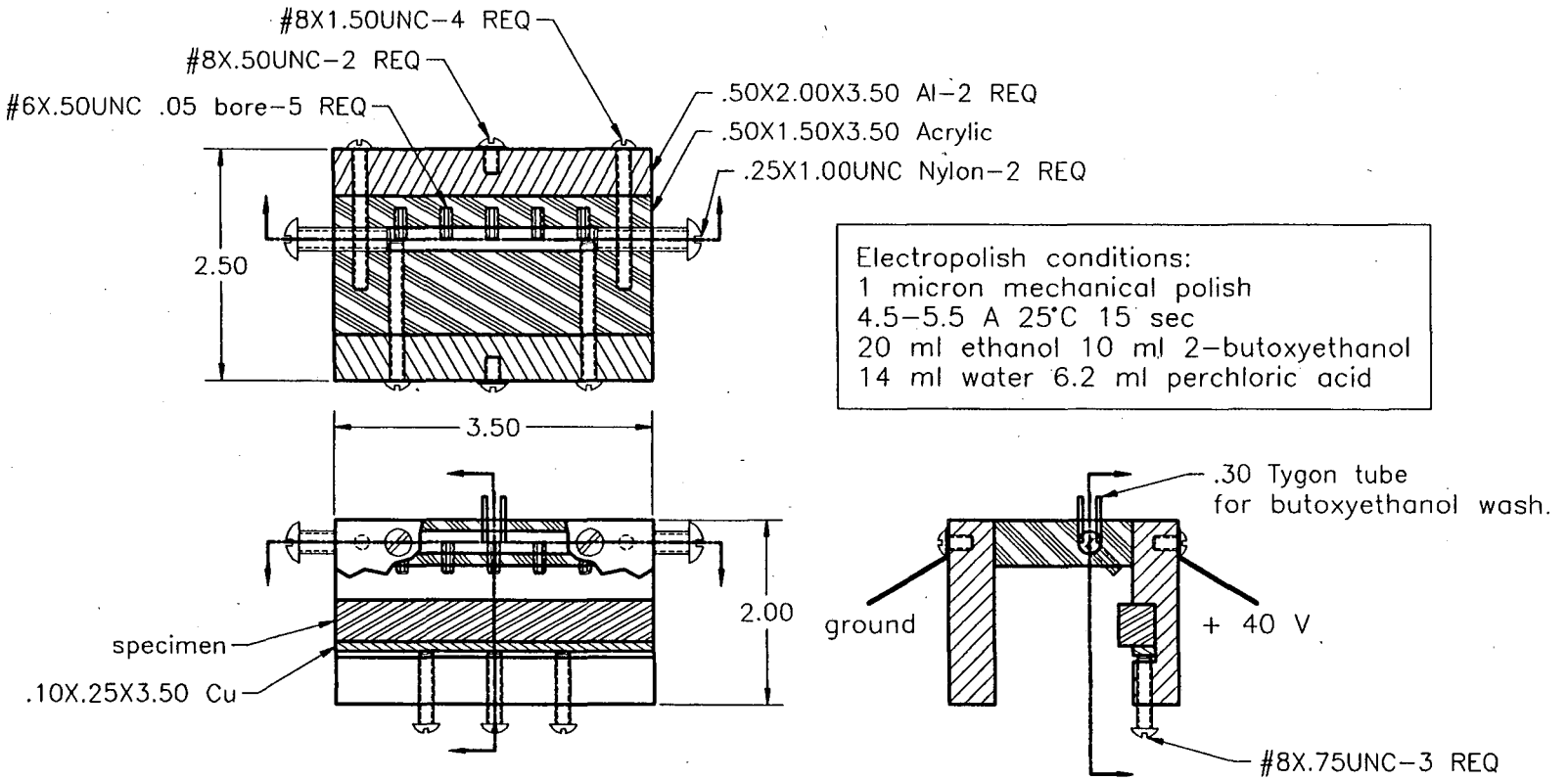

Figure 1: Design of electropolisher for large area specimens.

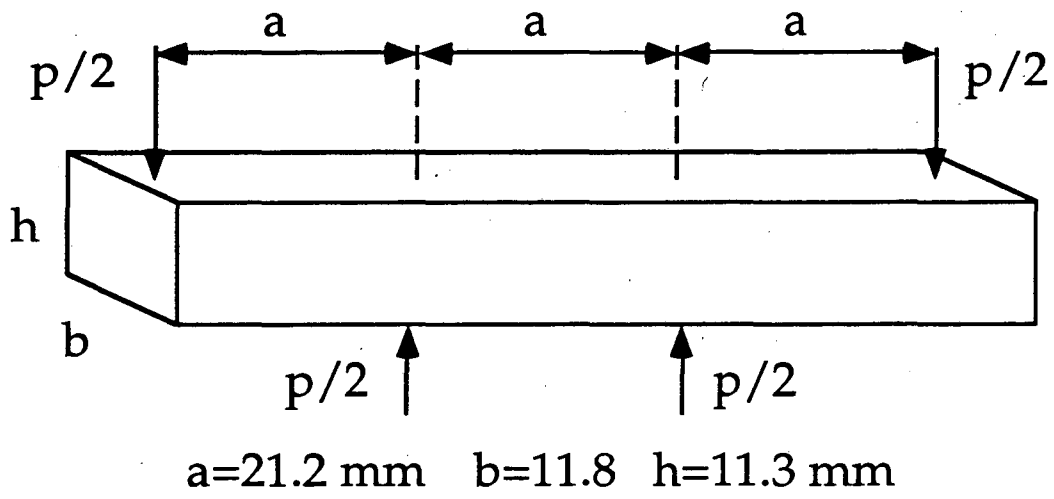

Figure 2: Loading configuration of four-point bending specimens.

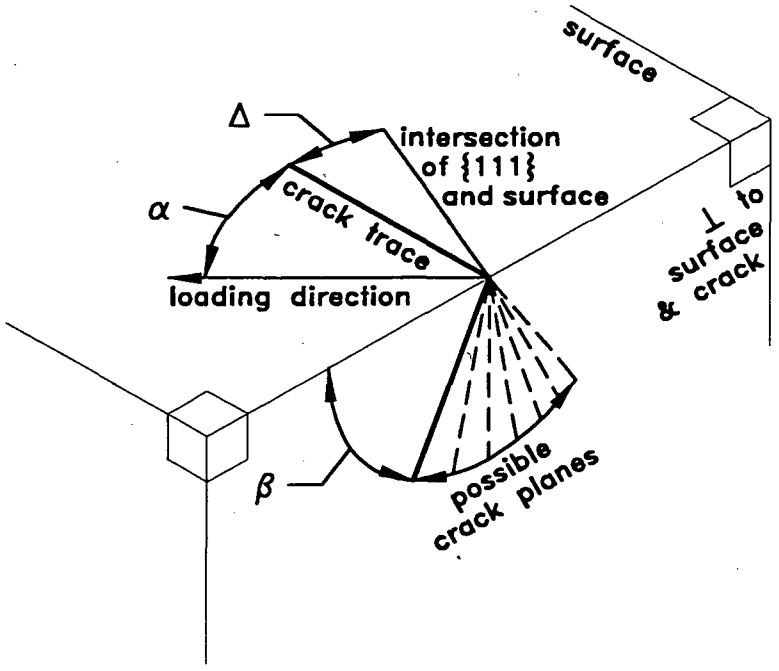

Figure 3: Diagram of the angle α between the crack trace and the tensile direction, the angle β between a given plane and the plane of the surface, and an angular deviation Δ between observed crack lines and one intersection of a {111} plane with the surface.

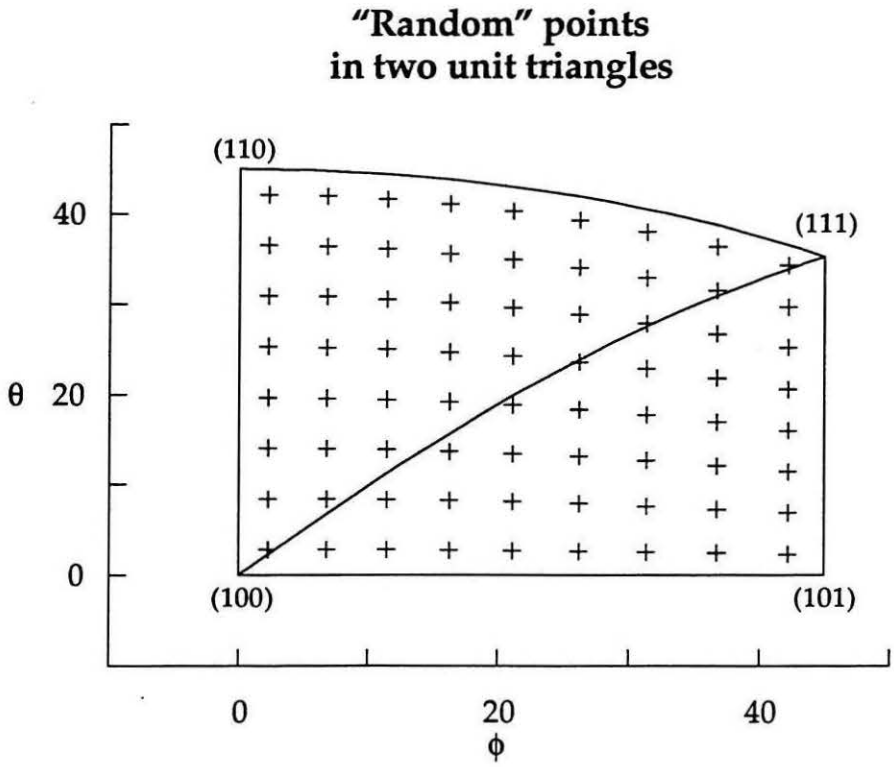

Figure 4: Plot of orientations of "random" grains within two unit crystallographic triangles.

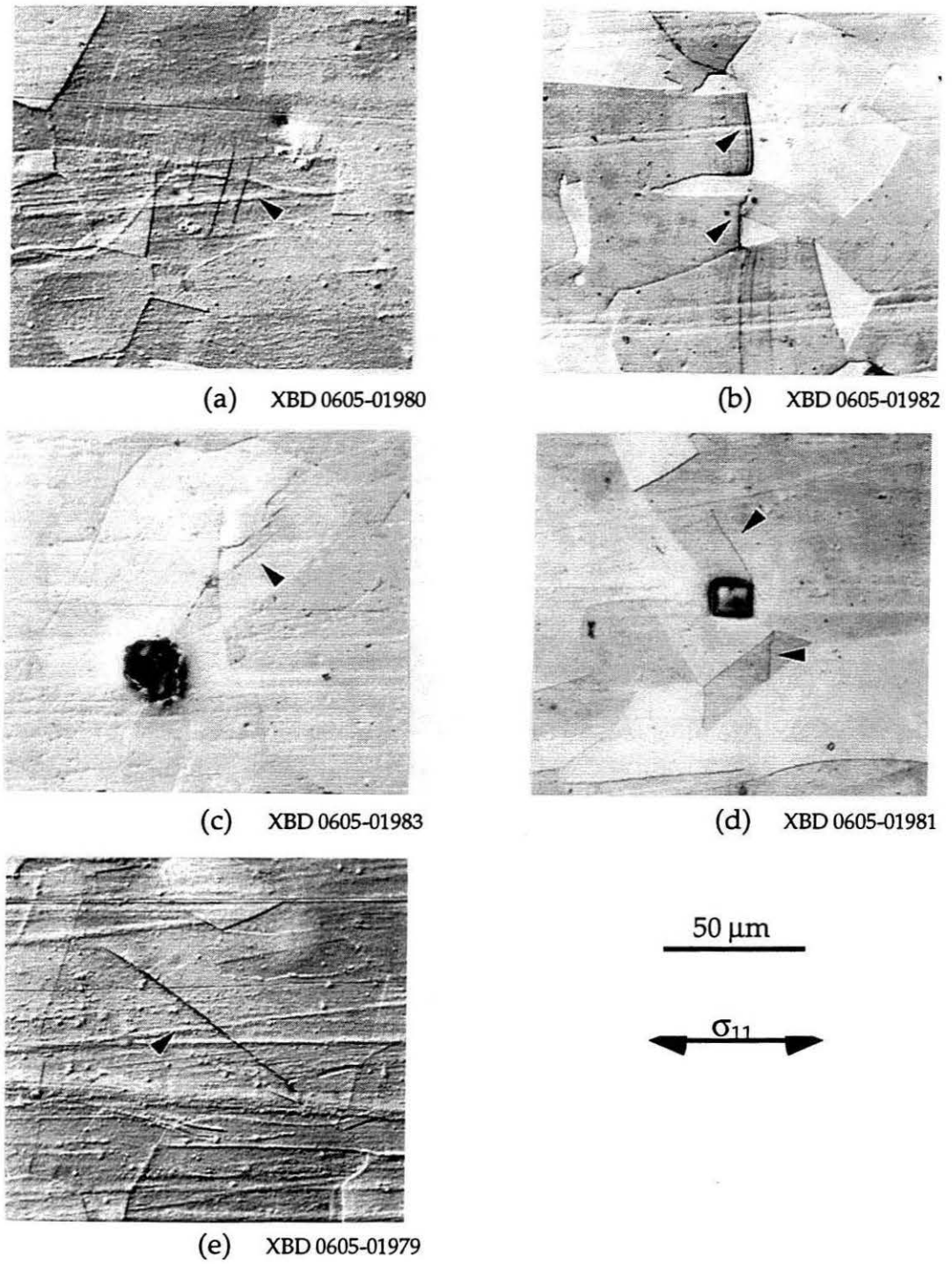

Figure 5: Fatigue crack initiation sites in I-908: (a) uncracked slip bands in grain well oriented for multiple slip, (b) isolated intergranular crack, (c) tortuous transgranular crack, (d) two sharp transgranular cracks initiating at inclusion (upper crack initiated first), and (e) isolated transgranular crack oriented for maximal shear

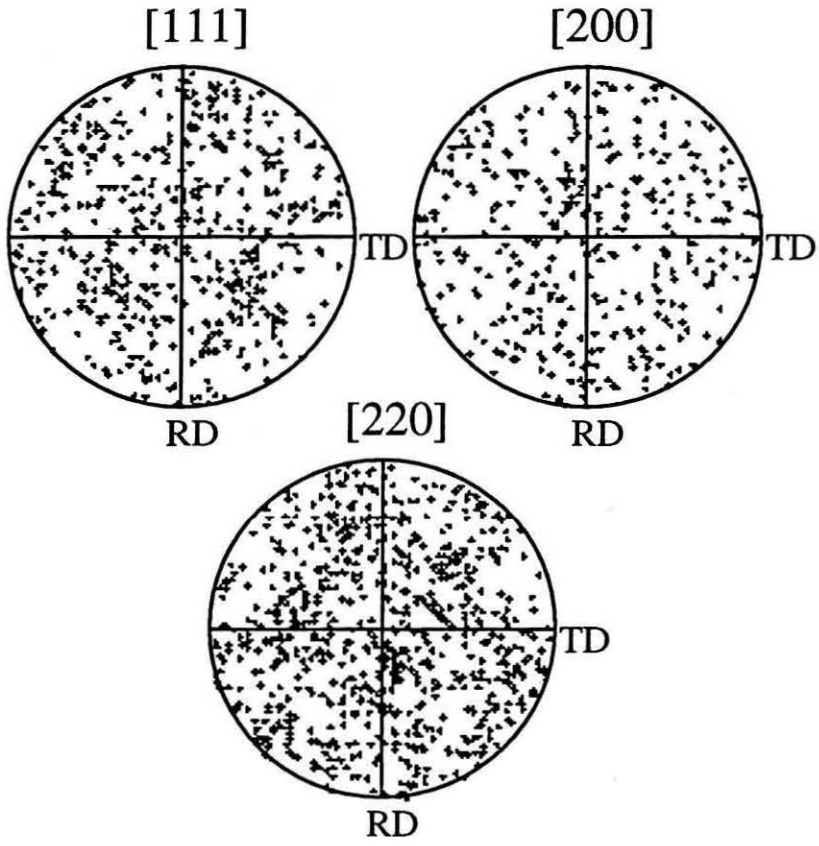

Figure 6: Discrete pole figures revealing no overall strong texture of I-908 specimen.

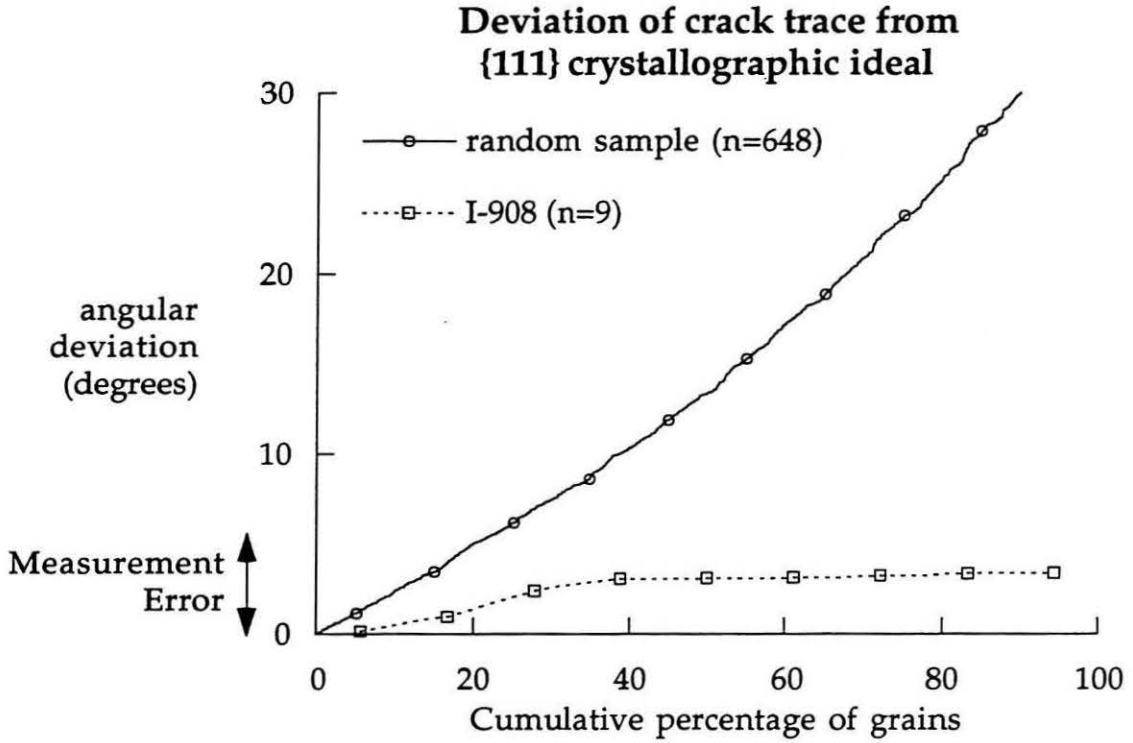

Figure 7: Distributions of deviations of crack traces from nearest {111} plane for cracked I-908 grains and a "random" set.

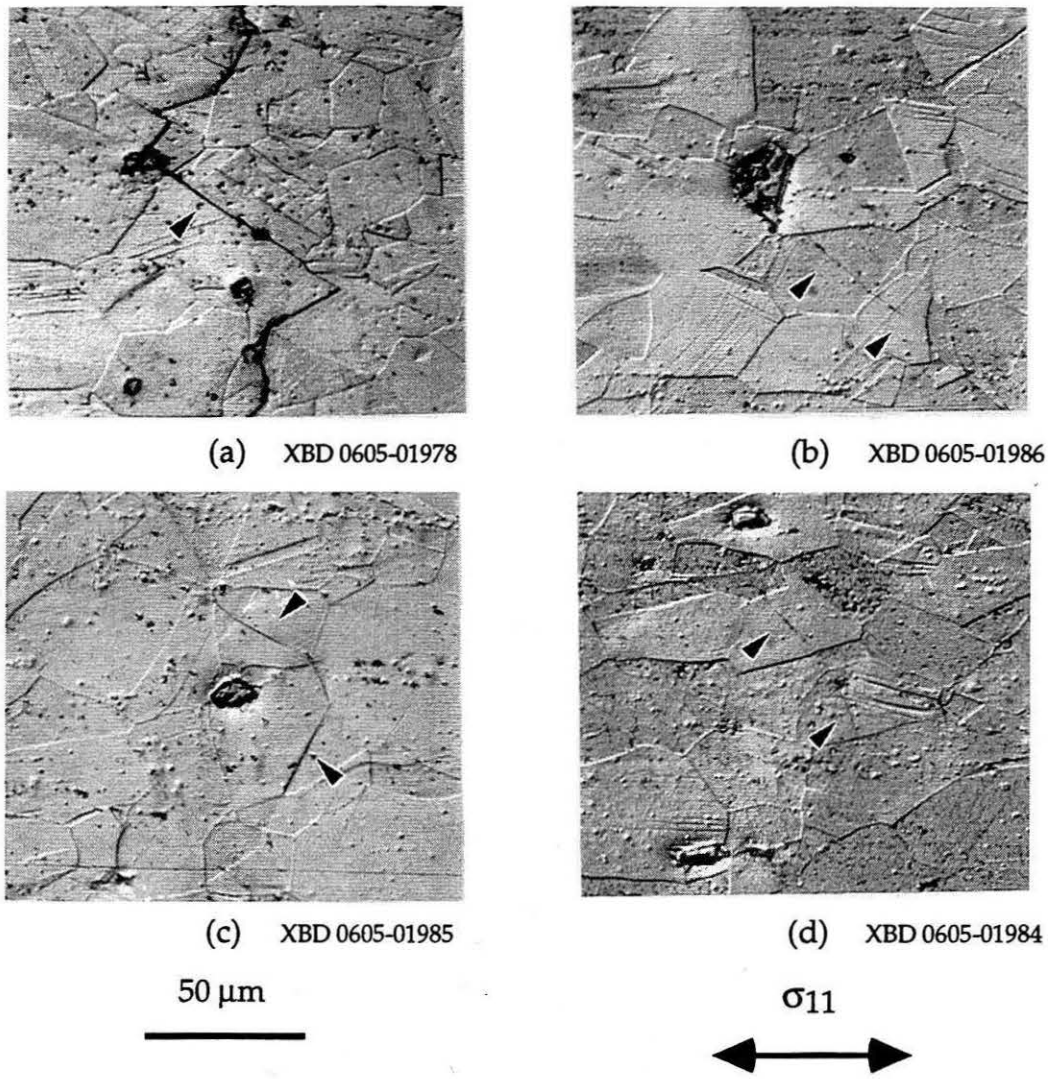

Figure 8: Fatigue crack initiation sites in A-286: (a) intergranular crack initiating at oxide inclusion, (b) transgranular crack near large inclusion, (c) transgranular (upper) and intergranular (lower) cracks initiating near inclusion, and (d) two isolated transgranular cracks.

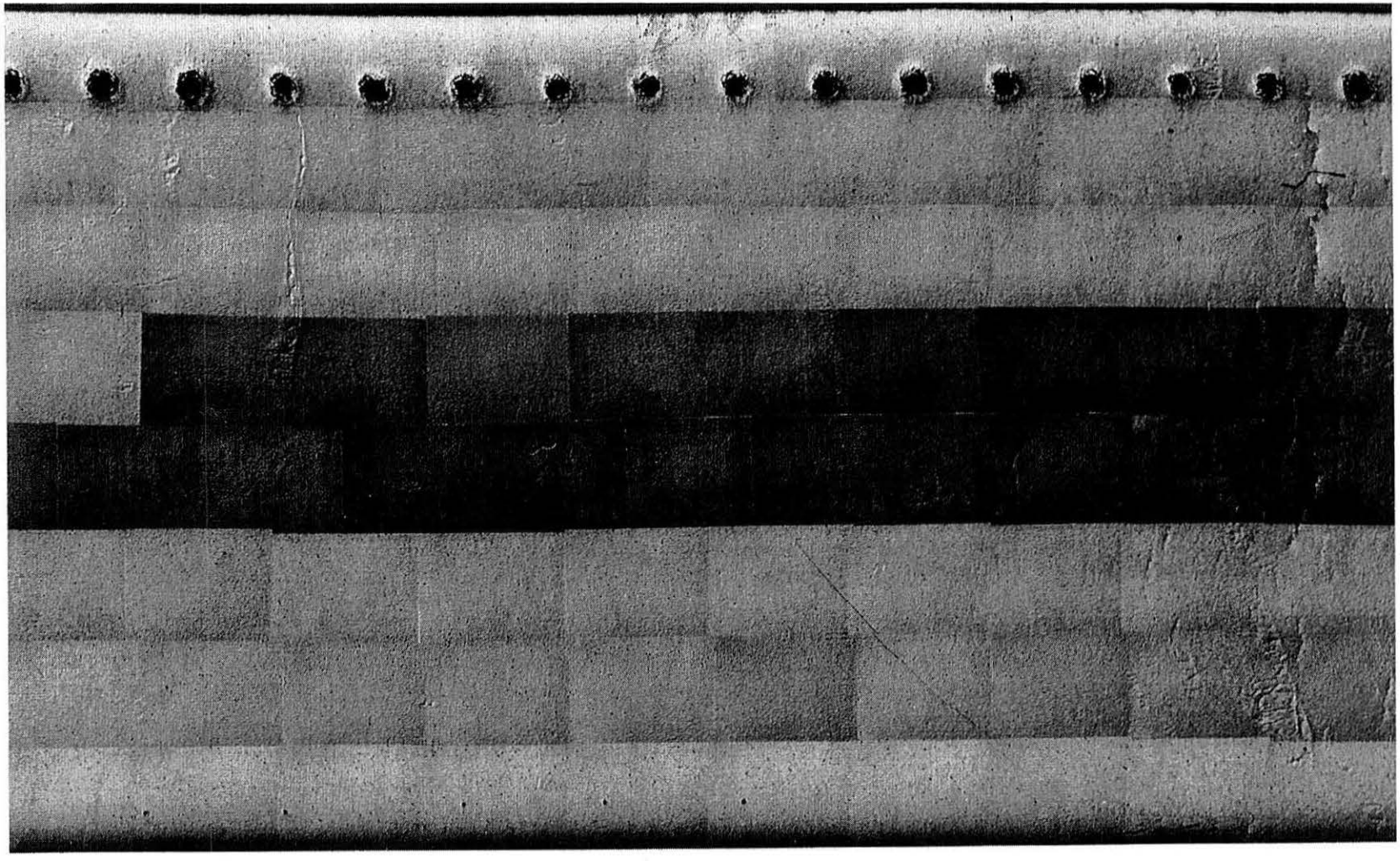

Figure 9a: Map of all recorded cracks in A-286: optical micrographs.
(XBB 964-1905)

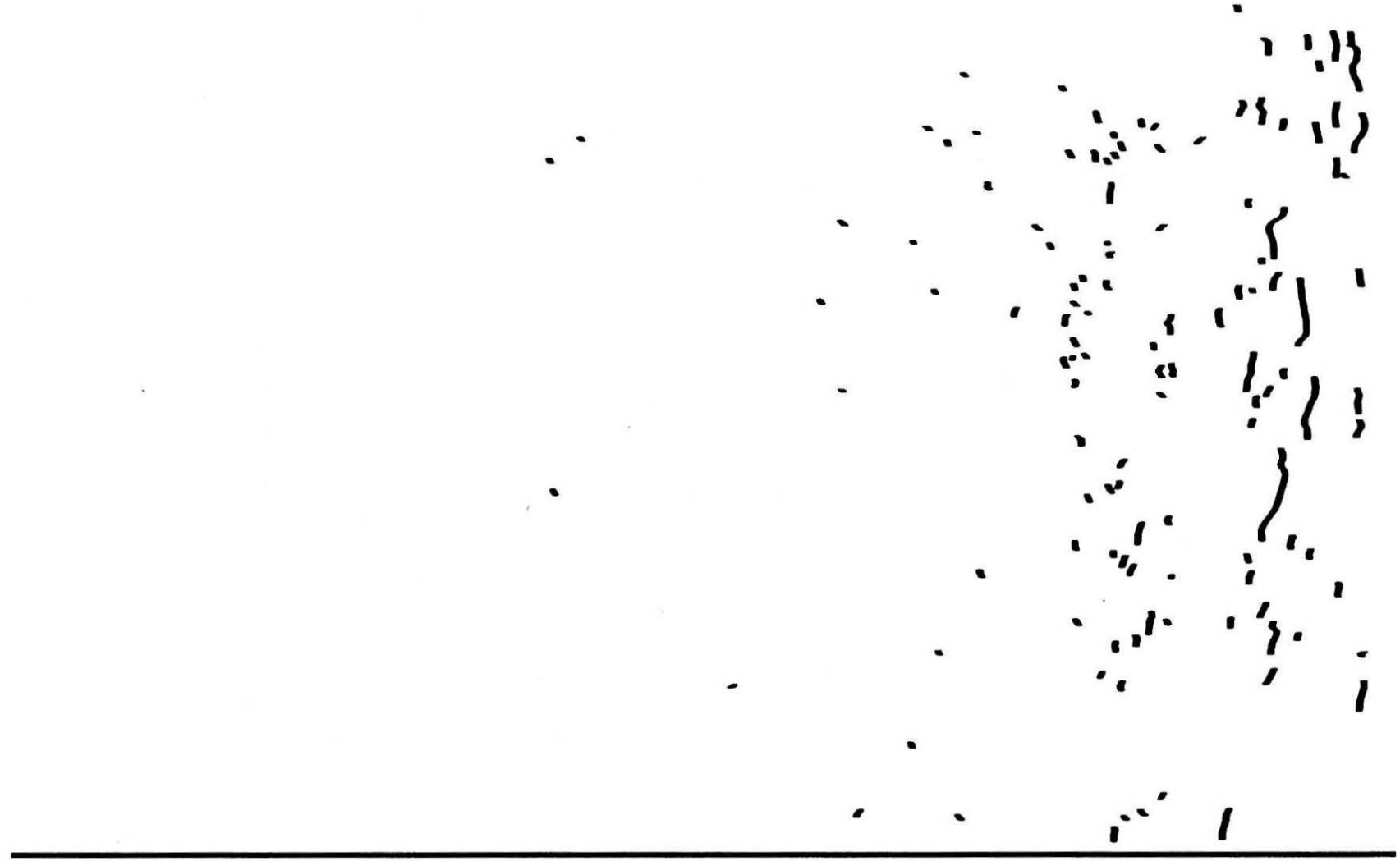

Figure 9b: Map of all recorded cracks in A-286: crack traces.

1 mm

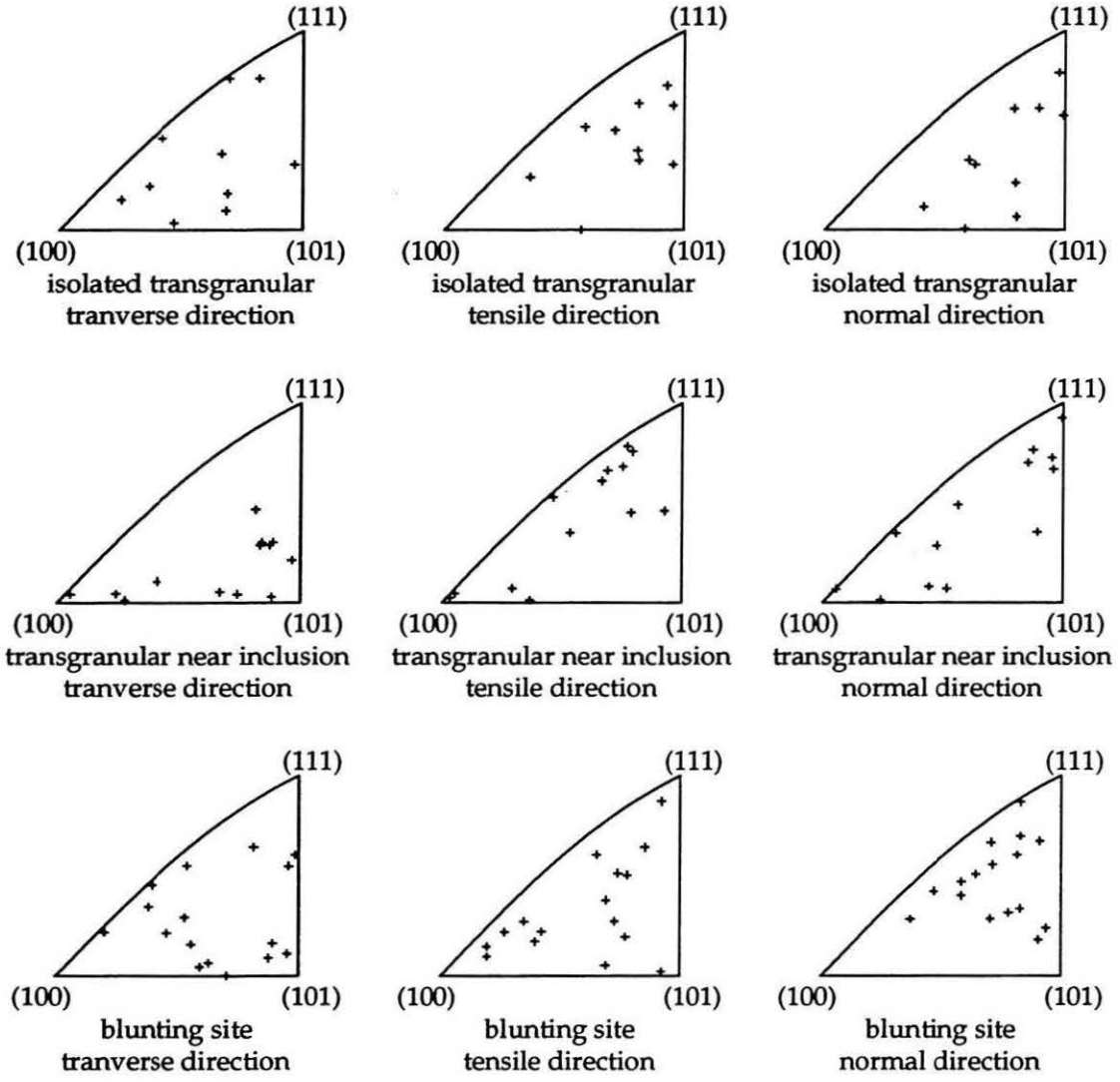

Figure 10: Inverse pole figures for initiation and blunting sites in A-286.

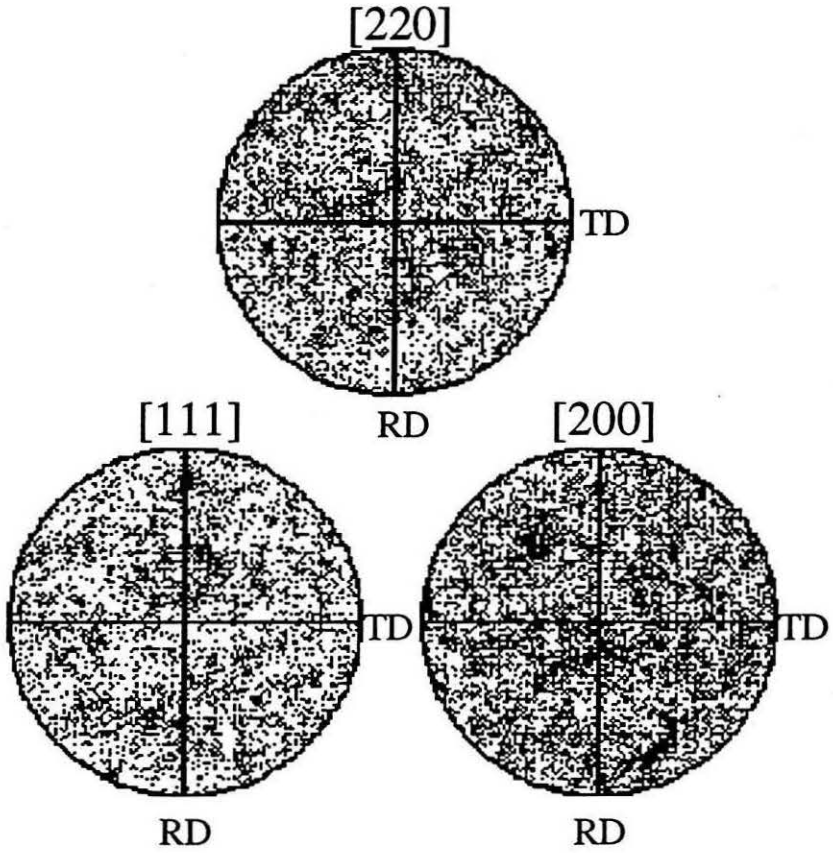

Figure 11: Discrete pole figures revealing no overall strong texture of A-286 specimen.

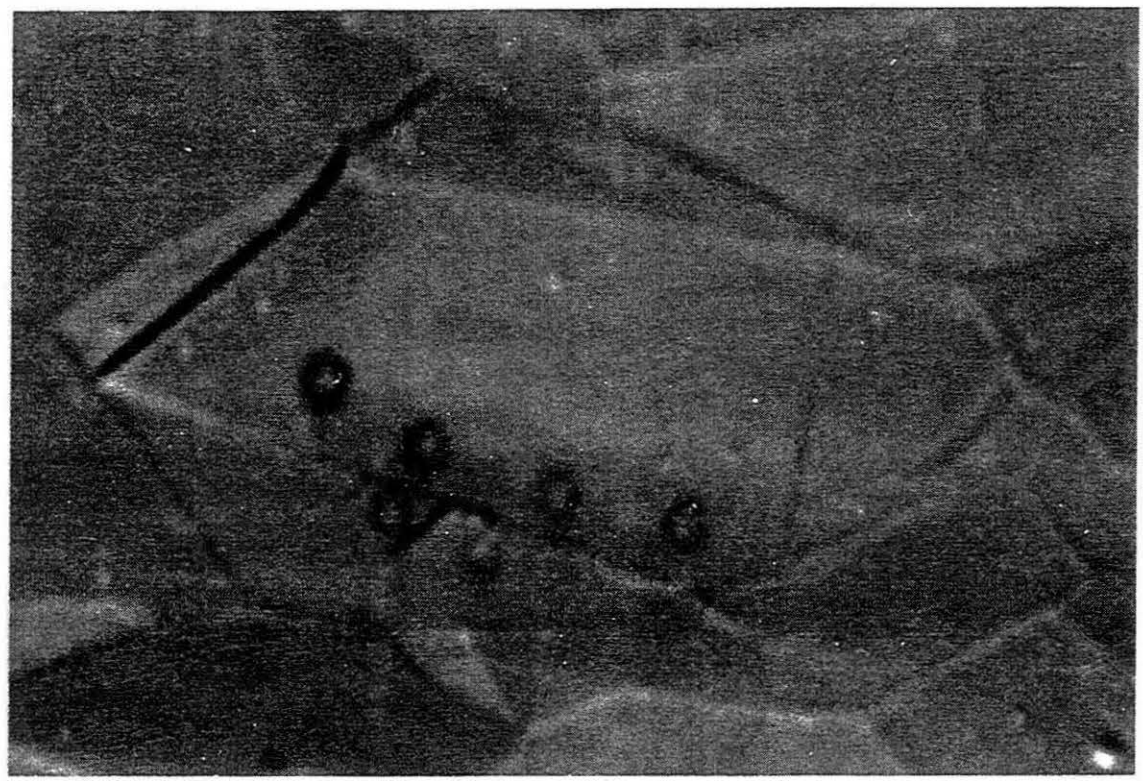

Figure 12a: Misorientation measurements in an incompletely cracked grain of A-286: SEM micrograph (XBD 9612-06204).

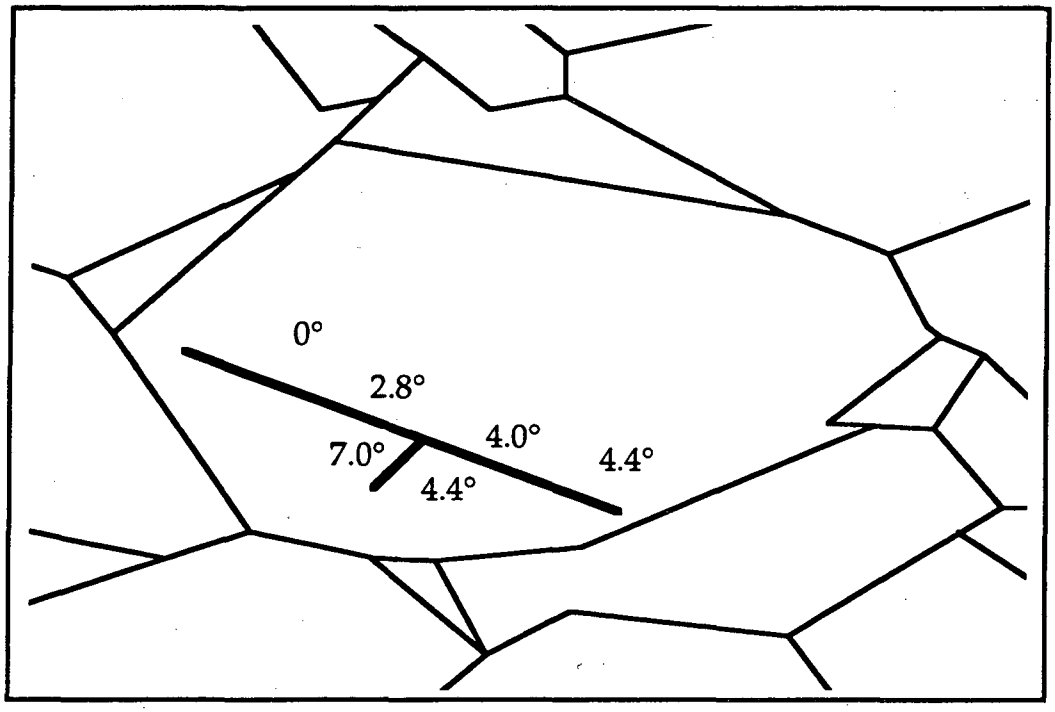

Figure 12b: Misorientation measurements in an incompletely cracked grain of A-286: schematic.

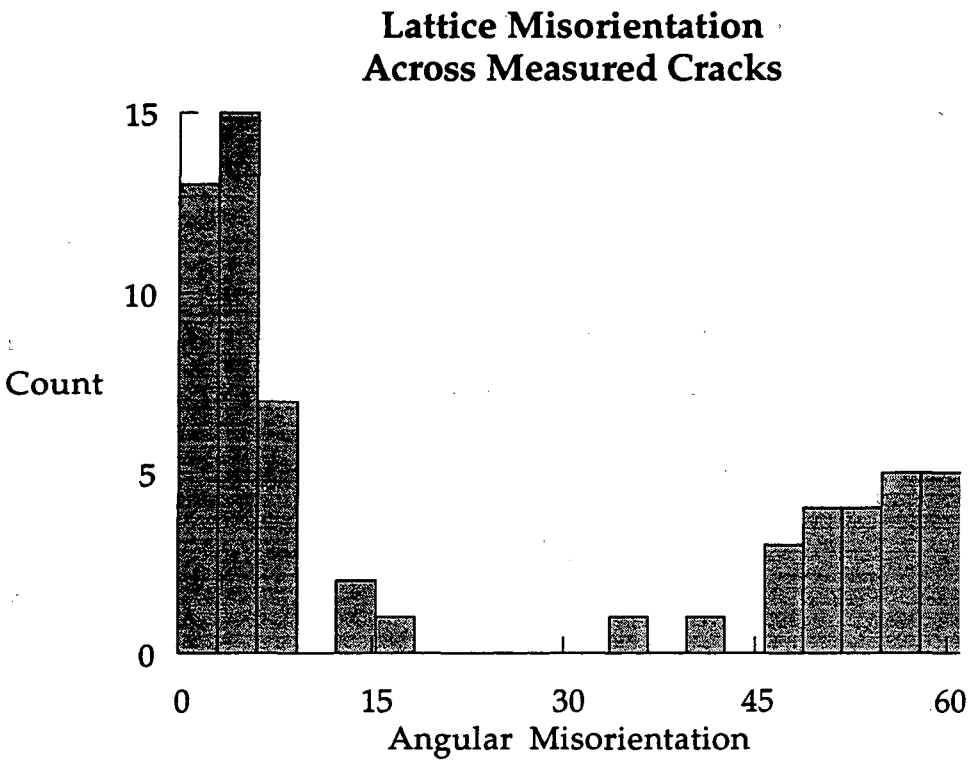

Figure 13: Histogram of lattice misorientations across measured cracks.

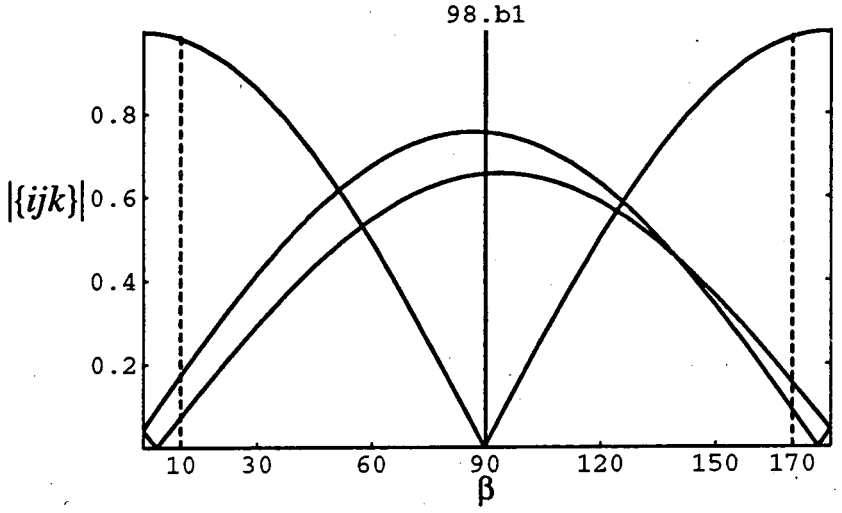

(a)

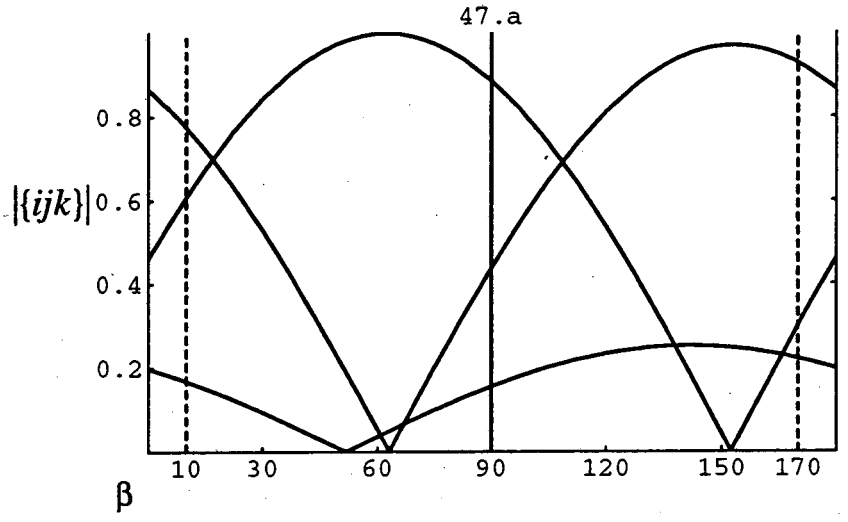

(b)

Figure 14: Plots of possible crack plane normals in A-286 as a function of β, the angle between the crack and surface normals. Notice (a) intersection of {110} (β ≅ 90°), {100} (β ≅ 0°), and symmetric {111} planes (β ≅ 50° & 125°), and (b) isolated {100} plane (β ≅ 60°).

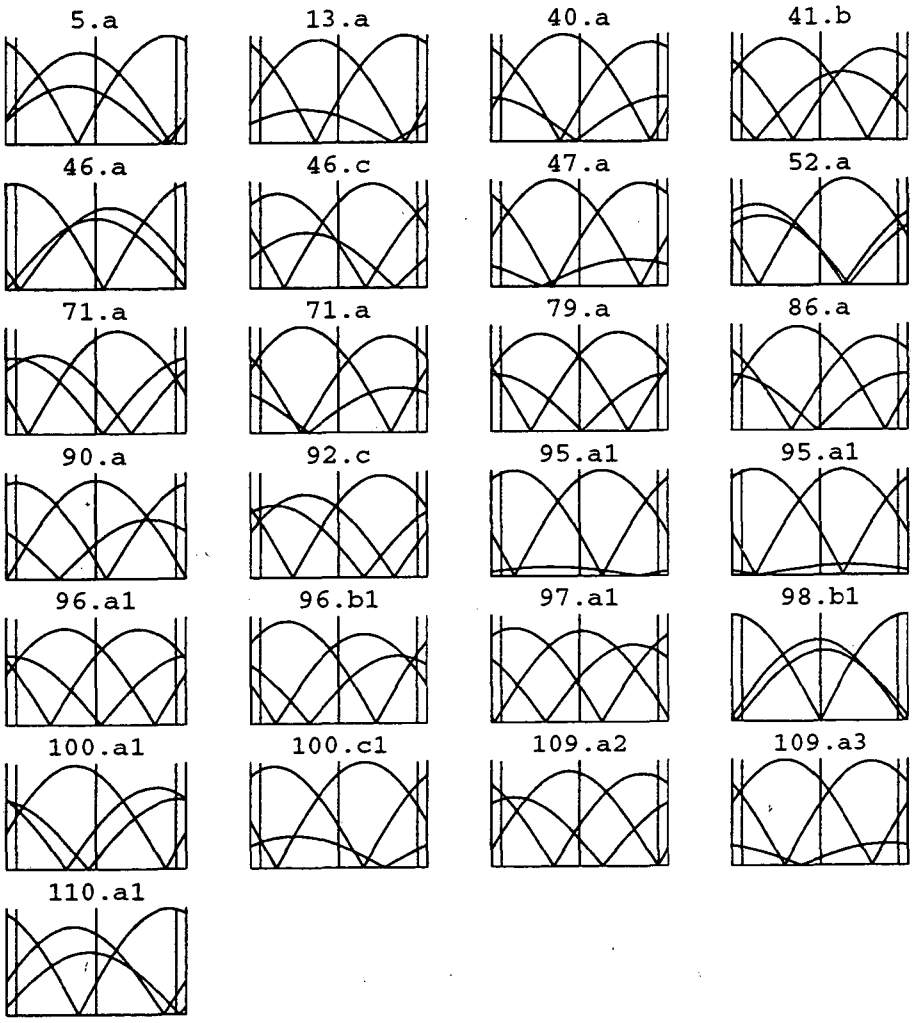

Angles α between crack traces and tensile direction

grain	α	grain	α	grain	α	grain	α
5.a	57	13.a	76	40.a	35	41.b	35
46.a	42	46.c	37	47.a	63	52.a	27
71.a1	24	71.a2	37	79.a	47	86.a	36
90.a	40	92.c	38	95.a1	54	95.a2	45
96.a1	46	96.b1	68	97.a	45	98.b1	50
100.a1	36	100.c1	60	109.a2	15	109.a3	52
110.a1	53						

Figure 15: Plots of possible crack plane normals in A-286.

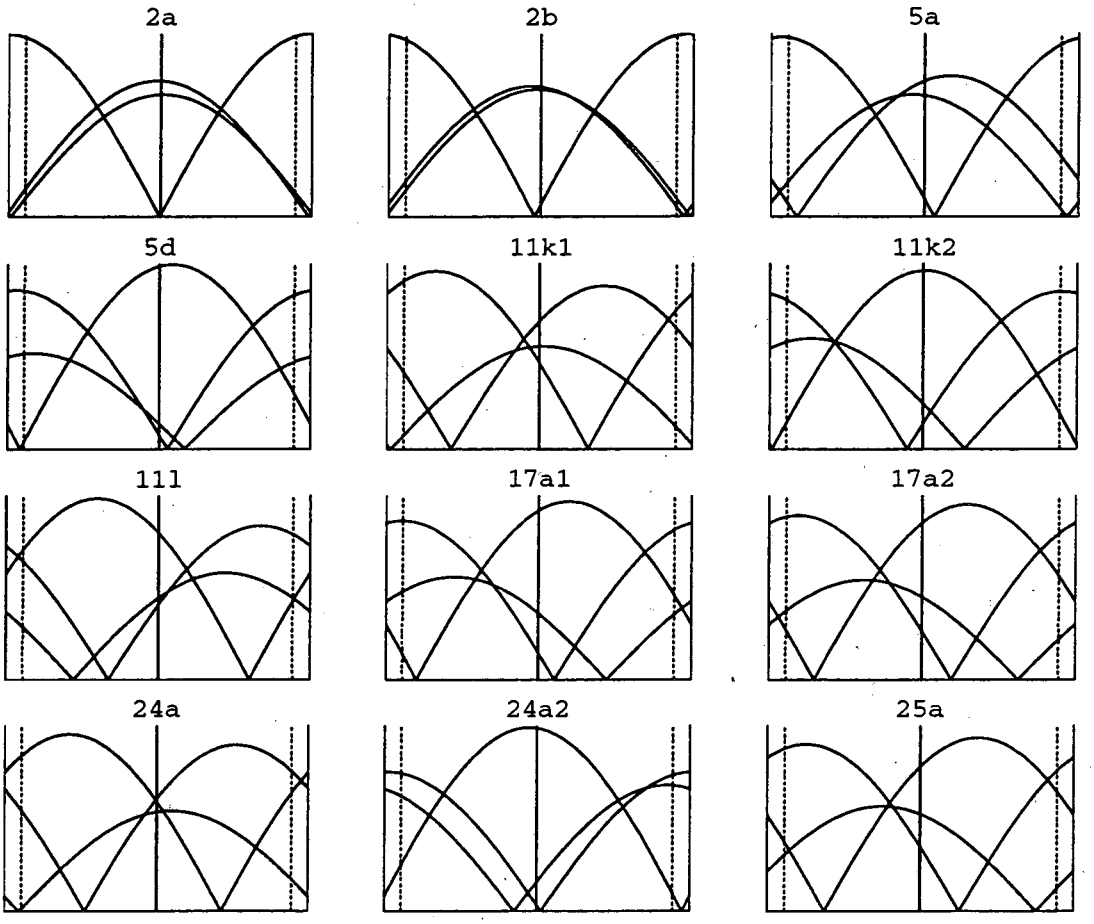

Angles α between crack traces and tensile direction

grain	α	grain	α	grain	α
2a	77	11k1	30	17a2	17
2b	73	11k2	78	24a	38
5a	58	111	47	24a2	28
5d	89	17a1	29	25a	35

Figure 16: Plots of possible crack plane normals in I-908, including 3 slip bands (2a, 2b, and 24a2).

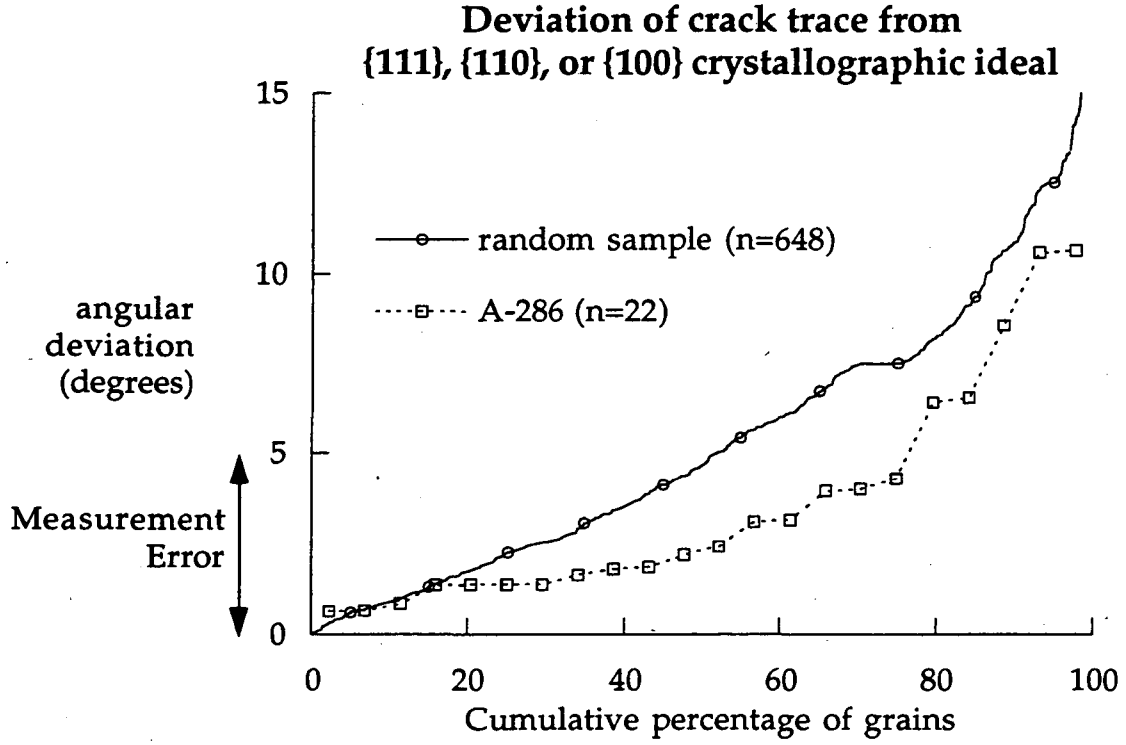

Figure 17: Distributions of deviations of crack traces from nearest {111}, {110}, or {100} plane for cracked A-286 grains and a "random" set.

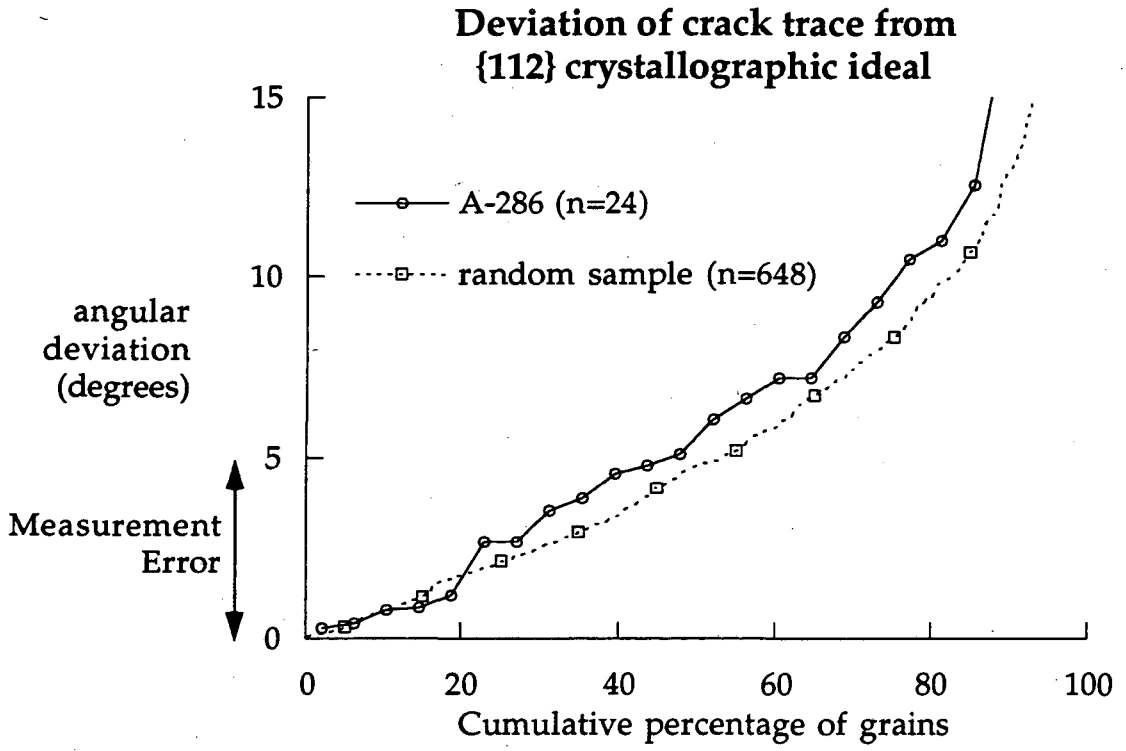

Figure 18: Distributions of deviations of crack traces from nearest {112} plane for cracked A-286 grains and a "random" set.

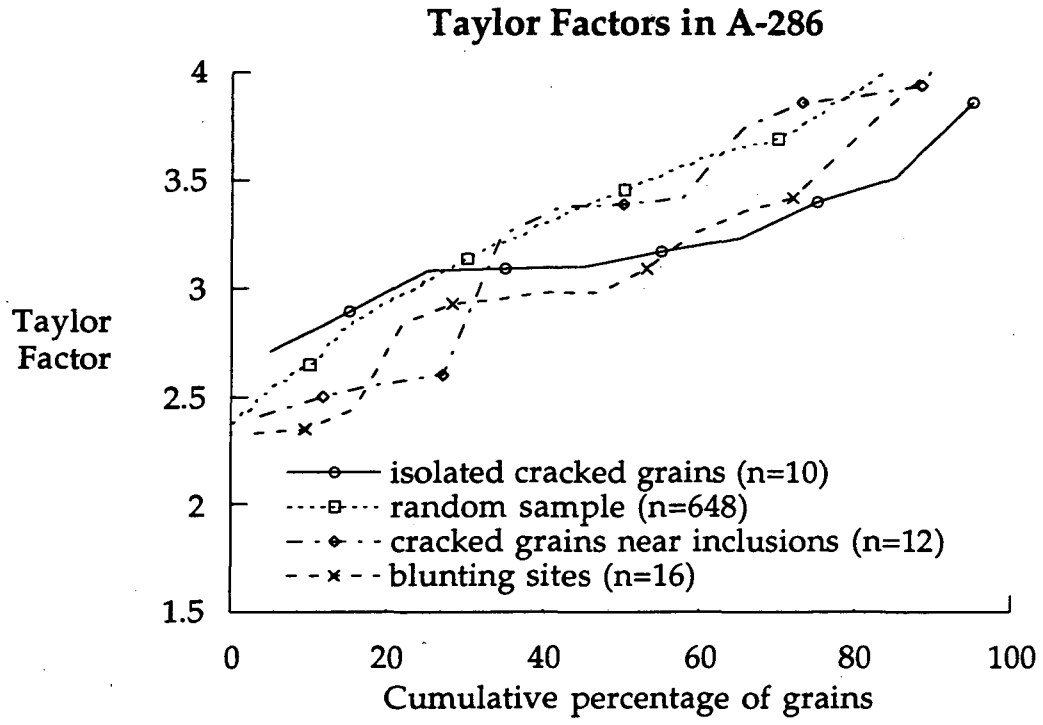

Figure 19: Distributions of calculated Taylor factors for cracked grains and blunting sites in A-286 as compared to a "random" set.

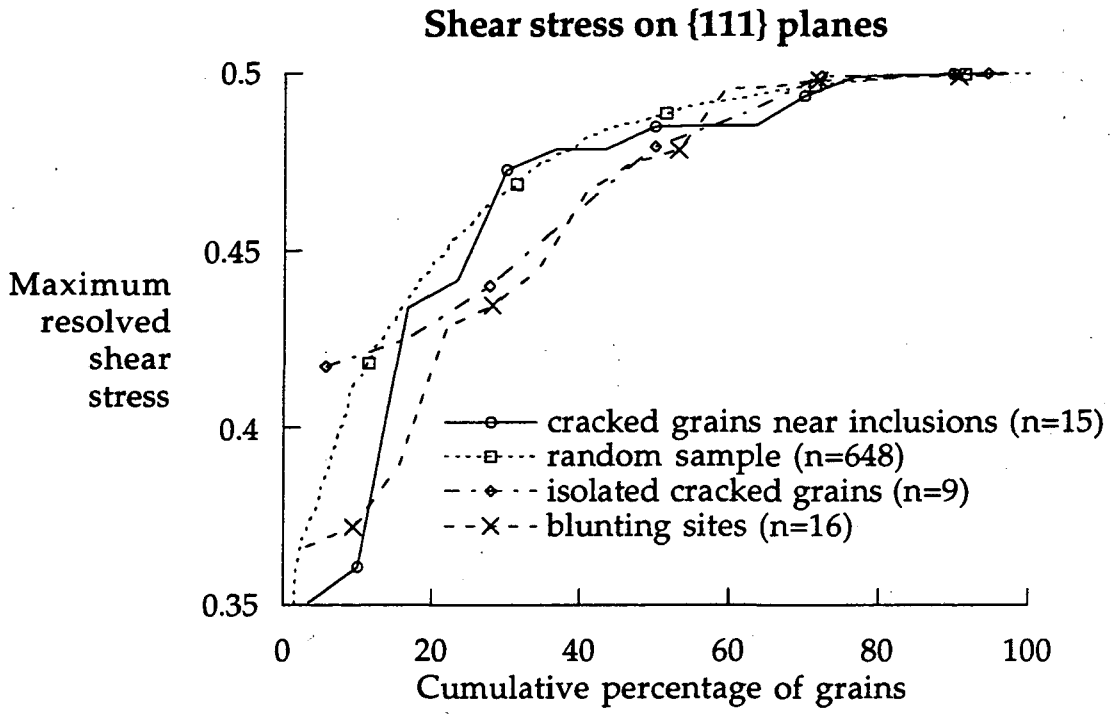

Figure 20: Distributions of maximum {111} resolved shear stresses for cracked grains and blunting sites in A-286 as compared to a "random" set.

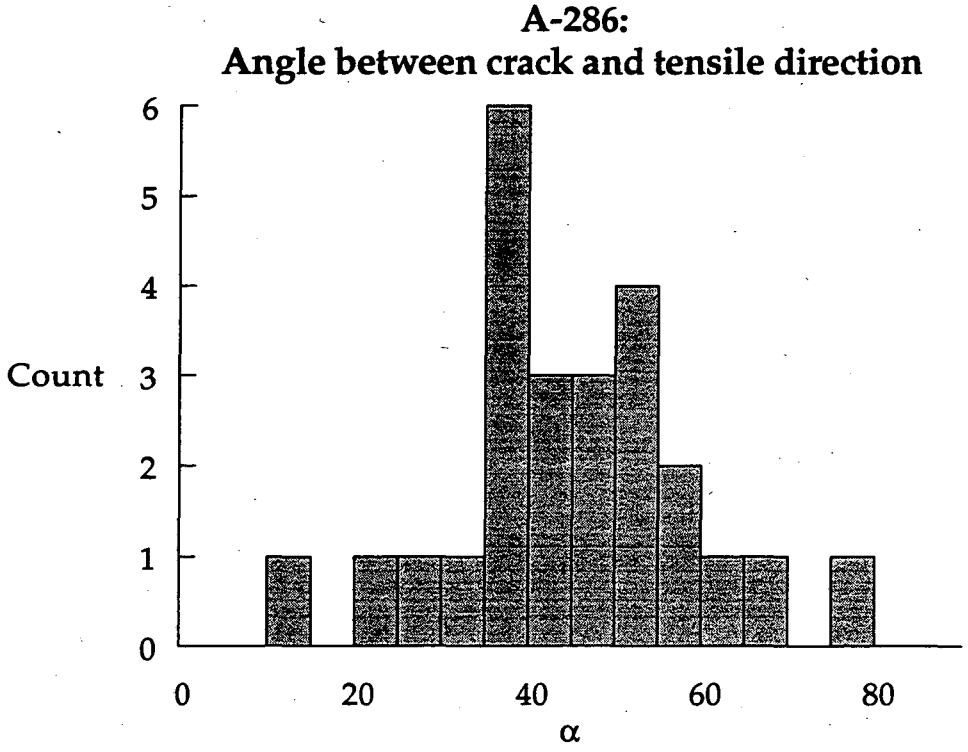

Figure 21: Histogram of observed angles between crack traces and tensile direction.

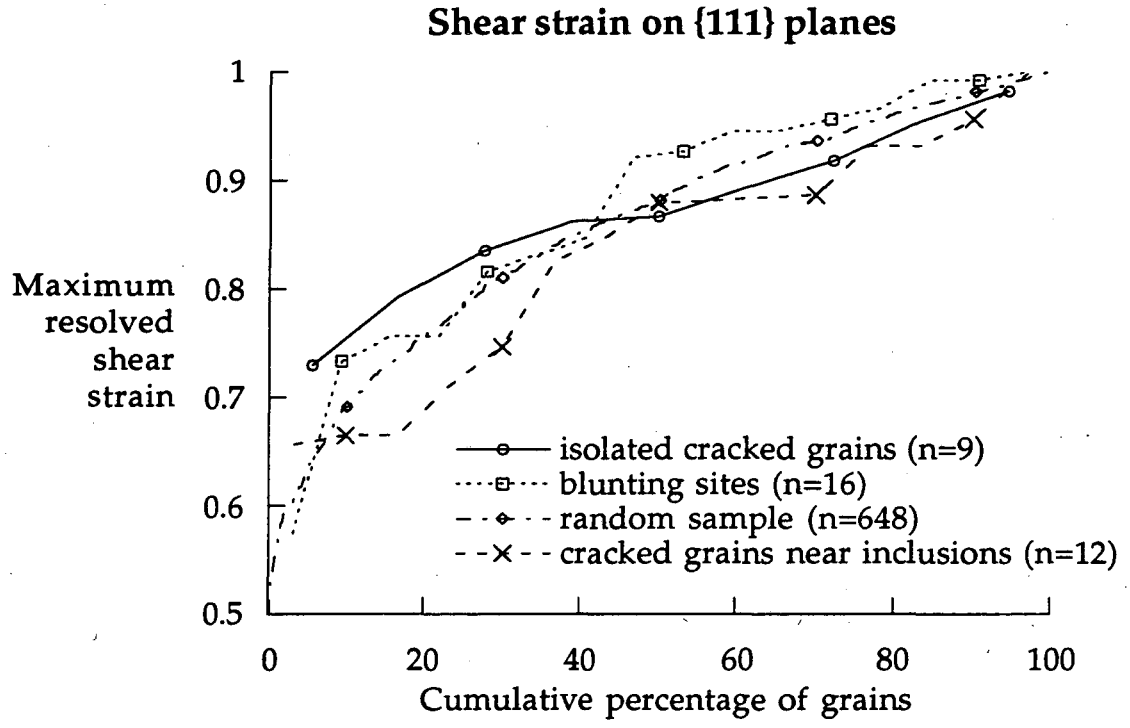

Figure 22: Distributions of maximum {111} resolved shear strains for cracked grains and blunting sites in A-286 as compared to a "random" set.

Appendix: FORTRAN Code

Calculation of grain misorientations

```
   Character*9 revdate
ccc
c  Program minang.f
c  by Tom Mason, Yale University, 1992.
c  minor revisions by Chris Krenn
   revdate = '4/1/96'
c
c  Program requires files 'VAXfunctions.f.o' and 'cubicsym.dat'
c  to be in working directory.
c
c       Input is expected to be list of pairs of:    grainname,3*3 matrix
c       Output is saved as list of:                  angle,grain1,grain2
c
c
c  To compile in the MPW environment, use:
c    F77 minang.f -w -W -tool -N9 -K -link VAXFunctions.f.o
c    link.out
c              VAXFunctions allows a date stamp
c              -W enables wide lines
c              -w ignores many compile errors
c              -K enables \t to print tabs
c              -N9 checks for cmd-. more often
c              -tool compiles code to run under MPW

ccc
c  Variables

   CHARACTER*30 fname
   character*10 grain1,grain2
   real*4 a(3,3),TRAN(24,3,3),b(3,3),tp(3,3)
   real*4 T(3,3),omega,trT,okeep,A1(3,3),A2(3,3)

   open(unit=9,file='cubicsym.dat')
   WRITE(*,*)' '
   WRITE(*,*) 'Enter name for misorientation matrices file.'
   READ(*,'(A)')fname
   OPEN(12,FILE=fname)
   WRITE(*,*) 'Enter name for output misorientation angle file.'
   READ(*,'(A)')fname
   OPEN(13,FILE=fname)

   ic=0
5  continue
ccc     READ ORIENTATION MATRICES INTO ARRAY

   read(12,*,end=500) grain1
   do 10 k=1,3
10 read(12,*,end=500)( a(k,il),il=1,3)

   read(12,*,end=500) grain2
   write(*,*) grain2
   do 12 k=1,3
12 read(12,*,end=500)( b(k,il),il=1,3)

   ic=ic+1
```

```
ccc     READ IN TRANSFORMATION MATRICES--24 3 X 3 MATRICES
   do 15 i=1,24
        read(9,*) z
        do 15 j=1,3
               read(9,*)(TRAN(i,j,k),k=1,3)
15      continue
   rewind(9)

   do 20 i=1,3
   do 20 j=1,3
20 tp(i,j)=0.0

cc sort to find minimum omega with respect
        to peak orientation

   okeep=1.570796327  ! 90 degrees
   do 242 n=1,24

   do 219 i=1,3
   do 219 j=1,3
        A2(i,j)=0.0
        do 219 k=1,3
        A2(i,j)=A2(i,j)+TRAN(n,i,k)*a(k,j)
219     continue

   do 242 ni=1,24

   do 220 i=1,3
   do 220 j=1,3
        A1(i,j)=0.0
        do 220 k=1,3
        A1(i,j)=A1(i,j)+TRAN(ni,i,k)*b(k,j)
220     continue

   do 240 i=1,3
   do 240 j=1,3
        T(i,j)=0.0
        do 240 k=1,3
        T(i,j)=T(i,j)+A2(i,k)*A1(j,k)
240     continue

   d1 = T(1,1)*(T(2,2)*T(3,3) - T(3,2)*T(2,3))
   d2 =-T(1,2)*(T(2,1)*T(3,3) - T(3,1)*T(2,3))
   d3 = T(1,3)*(T(2,1)*T(3,2) - T(3,1)*T(2,2))
   detT = d1+d2+d3

   trT=T(1,1)+ T(2,2)+ T(3,3)

   if (detT.lt.0.0) trT=-trT

   arg = (trT-1.0)/2.0

   omega=acos(arg)

   if(omega.lt.okeep)then
        okeep=omega

        do 38 i3=1,3
        do 38 j3=1,3
38      tp(i3,j3)=T(i3,j3)

   endif

242     continue
```

```
   write(13,*) okeep," \t ",grain1," \t ",grain2
   write(*,*) okeep

   go to 5
500    call date(datestr)
   write(13,*)
   write(13,*) "min ang, grain1, grain2"
   write(13,*) "Output on ",datestr," by minang.f rev. ",revdate
   stop
   end


c  file cub.sym.dat

1                          9                          17
 1  0  0                    0  0  1                   -1  0  0
 0  1  0                    1  0  0                    0  0 -1
 0  0  1                    0  1  0                    0 -1  0
2                          10                         18
-1  0  0                    0  0 -1                    1  0  0
 0 -1  0                    1  0  0                    0  0 -1
 0  0  1                    0 -1  0                    0  1  0
3                          11                         19
-1  0  0                    0  0 -1                    1  0  0
 0  1  0                   -1  0  0                    0  0  1
 0  0 -1                    0  1  0                    0 -1  0
4                          12                         20
 1  0  0                    0  0  1                   -1  0  0
 0 -1  0                   -1  0  0                    0  0  1
 0  0 -1                    0 -1  0                    0  1  0
5                          13                         21
 0  1  0                    0  0 -1                    0 -1  0
 0  0  1                    0 -1  0                   -1  0  0
 1  0  0                   -1  0  0                    0  0 -1
6                          14                         22
 0 -1  0                    0  0  1                    0  1  0
 0  0  1                    0 -1  0                   -1  0  0
-1  0  0                    1  0  0                    0  0  1
7                          15                         23
 0  1  0                    0  0  1                    0  1  0
 0  0 -1                    0  1  0                    1  0  0
-1  0  0                   -1  0  0                    0  0 -1
8                          16                         24
 0 -1  0                    0  0 -1                    0 -1  0
 0  0 -1                    0  1  0                    1  0  0
 1  0  0                    1  0  0                    0  0  1
```

Calculation of Taylor factors

```
   Character*9 revdate
ccc
c  Program Bishop_Hill.f
c  by Chris Krenn
   revdate = '4/20/95'
c
c  Program requires files 'bishop_hill_data' and 'VAXfunctions.f.o'
c       to be in working directory.
c  bishop_hill_data lists 56 corner stress states that activate 6 or 8 slip systems
c       with a resolved shear stress of 1.
c
c       The state to first cause deformation will be the one that maximizes
c       Eij Sij in the crystal frame. The Taylor factor M is :
c
c M = (Sigma)xx / Tau = Sum d (Gamma)i/ d (Epsilon)xx = dw / (Tau * d (Epsilon)xx)
c
c  Ref: Bishop and Hill, Phil Mag 1951, vol. 42, pp. 1298-1307
c       G.Y. Chin et. al., Acta Met, vol. 14, 467-476
c       and B.L. Adams class notes, Yale University, 1992
c
c Input is expected to be list of:  phi1,phi,phi2,x,x,x,x,grainname
c Output is saved as list of:       M,grainname,active stress state,phi1,phi,phi2
c
c  program currently assumes plane strain in the +010 and -100 directions
c
c
c  To compile in the MPW environment, use:
c    F77 bishop_hill.f -w -W -tool -N9 -K -link VAXFunctions.f.o
c    link.out
c               VAXFunctions allows a date stamp
c               -W enables wide lines
c               -w ignores many compile errors
c               -K enables \t to print tabs
c               -N9 checks for cmd-. more often
c               -tool compiles code to run under MPW

ccc
c  Variables

c  input from disk, keyboard
   CHARACTER*30 fname
   CHARACTER*10 grain
   CHARACTER*9 datestr
   character*1 debug
   real*4 phi1,phi2,phi,g(3,3)
   real*4 x1,x2,x3,x4
c  bishop hill stresses
   real*4 bhs (3,3,56),a1,a2,a3,a4,a5,a6,s6

c  calculation: maxwork, taylor factor
   real*4 labe(3,3), xle(3,3), dw, dwmax, mfac, esum
   real*4 a,b,f,g2,h
   integer bestsys, s
```

```
ccc
c  user input

   WRITE(*,*)' '
   WRITE(*,*) 'Enter name for grain orientation file.'
   READ(*,*) fname
   OPEN(unit=1, file=fname, status='old')
   WRITE(*,*) 'Enter name for output taylor factor data'
   READ(*,*) fname
   OPEN(unit=2,file=fname, status='new')

   WRITE(*,*) 'Print matrices (Y/N)'
   READ(*,*) debug

ccc
c  initialize:

c       read corner stress states
   OPEN(unit=3, file='bishop_hill_data', status='old')

   s6 = sqrt(6.0)/2
   Do 20 i = 1,56
     read (3,*) a1,a2,a3,a4,a5,a6
     bhs (1,1,i) = a1*s6
     bhs (2,2,i) = a2*s6
     bhs (3,3,i) = a3*s6
     bhs (2,3,i) = a4*s6
     bhs (3,2,i) = a4*s6
     bhs (1,3,i) = a5*s6
     bhs (3,1,i) = a5*s6
     bhs (1,2,i) = a6*s6
     bhs (2,1,i) = a6*s6
20 Continue
   close(3)

c  lab strain
   data labe /-.01,0,0, 0,.01,0, 0,0,0/

ccc
c  Main program

c  ***** read grain and euler angles
25 read(1,*, end=130) phi1,phi,phi2,x1,x2,x3,x4,grain
   if (debug=='y') write(*,*) phi1,phi,phi2,x1,x2,x3,x4,grain

        g(1,1)=cos(phi1)*cos(phi2)-sin(phi1)*sin(phi2)*cos(phi)
        g(1,2)=sin(phi1)*cos(phi2)+cos(phi1)*sin(phi2)*cos(phi)
        g(1,3)=sin(phi2)*sin(phi)
        g(2,1)=-cos(phi1)*sin(phi2)-sin(phi1)*cos(phi2)*cos(phi)
        g(2,2)=-sin(phi1)*sin(phi2)+cos(phi1)*cos(phi2)*cos(phi)
        g(2,3)=cos(phi2)*sin(phi)
        g(3,1)=sin(phi1)*sin(phi)
        g(3,2)=-cos(phi1)*sin(phi)
        g(3,3)=cos(phi)

c  transform strain to crystal frame
                     Do 40 i=1,3
                     Do 40 j=1,3
                            xle(i,j)=0.0
                            Do 30 m=1,3
                            Do 30 n=1,3
              xle(i,j)=xle(i,j) + 1.0*labe(m,n)*g(m,i)*g(n,j)
30                          Continue
40                   Continue
```

```
c   pick stress with max resultant work
    dwmax = 0.0
    do 90 s=1,56
         dw = 0.0
         do 50 i=1,3
           do 50 j = 1,3
             dw = dw + bhs(i,j,s) * xle(i,j)
50       continue
         if (dw > dwmax) then
           dwmax = dw
           bestsys = s
         endif
90  Continue
    if (debug=='y') then
      write(*,*) 'grain: ',grain
      write(*,*) 'system: ',bestsys
      write(*,*) 'max work:', dwmax
    endif


cc   calculate M
c
    a = bhs(2,2,bestsys) - bhs(3,3,bestsys)
    b = bhs(3,3,bestsys) - bhs(1,1,bestsys)
    f = bhs(2,3,bestsys)
    g2 = bhs(3,1,bestsys)
    h = bhs(1,2,bestsys)
    mfac = -b * xle(1,1) + a * xle(2,2) + 2 * f * xle(2,3)
    mfac = (mfac + 2 * g2 * xle(3,1) + 2 * h * xle(1,2))/labe(2,2)

c   output euler, M, system
    write(2,*) mfac," \t ",grain," \t ",bestsys," \t ",phi1," \t ",phi," \t ",phi2
    if (debug == 'y') then
      write(*,*) mfac,grain,bestsys,phi1,phi,phi2
    endif

    goto 25

c write footer on file
130     call date(datestr)
    write(2,*)
    write(2,*) "mfac, grainname, Bishop system, phi1,phi,phi2"
    write(2,*) "applied strain (Eii):", (labe(i,i),i=1,3)
    write(2,*) "Output on ",datestr," by bishop_hill.f rev. ",revdate
    if (debug == 'y') then
      write(*,*)
      write(*,*) "mfac, grainname, Bishop system, phi1,phi,phi2"
      write(*,*) "applied strain (Eii):", (labe(i,i),i=1,3)
      write(*,*) "Output on ",datestr," by bishop_hill.f rev. ",revdate
    endif
    close(2)
    close(1)

    end
```

```
c  file bishop_hill_data

(* list of 56 Bishop Hill Stress corner states,
    normalized to give resolved shear stresses of 1
    on sets of 6 or 8 slip systems. Stresses stored
    in 11,22,33,23,13,12 order.*)

0     0     -2.   0     0     0          0     1.    0     1.    0     -1.
0     2.    0     0     0     0          0     1.    0     1.    0     1.
0     0     2.    0     0     0          0     1.    0     -1.   0     -1.
0     -2.   0     0     0     0          0     1.    0     -1.   0     1.
-2.   0     0     0     0     0          0     0     1.    -1.   1.    0
2.    0     0     0     0     0          0     0     1.    1.    1.    0
0     0     0     2.    0     0          0     0     1.    -1.   -1.   0
0     0     0     0     2.    0          0     0     1.    1.    -1.   0
0     0     0     0     0     2.         0     -1.   0     -1.   0     1.
0     0     0     -2.   0     0          0     -1.   0     1.    0     1.
0     0     0     0     -2.   0          0     -1.   0     -1.   0     -1.
0     0     0     0     0     -2.        0     -1.   0     1.    0     -1.
-1.   1.    0     0     0     1.         0     1.    1.    0     1.    -1.
1.    0     -1.   0     1.    0          0     1.    1.    0     1.    1.
0     -1.   1.    1.    0     0          0     1.    1.    0     -1.   -1.
-1.   1.    0     0     0     -1.        0     1.    1.    0     -1.   1.
1.    0     -1.   0     -1.   0          0     -1.   -1.   0     -1.   1.
0     -1.   1.    -1.   0     0          0     -1.   -1.   0     1.    1.
1.    -1.   0     0     0     -1.        0     -1.   -1.   0     -1.   -1.
-1.   0     1.    0     -1.   0          0     -1.   -1.   0     1.    -1.
0     1.    -1.   -1.   0     0          0     0     0     1.    1.    -1.
1.    -1.   0     0     0     1.         0     0     0     1.    -1.   1.
-1.   0     1.    0     1.    0          0     0     0     -1.   1.    1.
0     1.    -1.   1.    0     0          0     0     0     1.    -1.   -1.
0     0     -1.   1.    -1.   0          0     0     0     -1.   1.    -1.
0     0     -1.   1.    1.    0          0     0     0     -1.   -1.   1.
0     0     -1.   -1.   -1.   0          0     0     0     1.    1.    1.
0     0     -1.   -1.   1.    0          0     0     0     -1.   -1.   -1.
```

Ernest Orlando Lawrence Berkeley National Laboratory
One Cyclotron Road | Berkeley, California 94720

Prepared for the U.S. Department of Energy under Contract No. DE-AC03-76SF00098